

**DEFECTS IN TITANIUM DIOXIDE: THEORY AND
COMPUTATIONS**

Sutassana Na Phattalung

**A Thesis Submitted in Partial Fulfillment of the Requirements for the
Degree of Master of Science in Physics
Suranaree University of Technology**

Academic Year 2006

ISBN 974-533-578-9

การศึกษาความบกพร่องในไทเทเนียมไดออกไซด์เชิงทฤษฎีและเชิงคำนวณ

นางสาวสุทัตนา ฅ พัทลุง

วิทยานิพนธ์นี้เป็นส่วนหนึ่งของการศึกษาตามหลักสูตรปริญญาวิทยาศาสตรมหาบัณฑิต

สาขาวิชาฟิสิกส์

มหาวิทยาลัยเทคโนโลยีสุรนารี

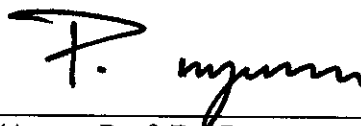
ปีการศึกษา 2549

ISBN 974-533-578-9

DEFECTS IN TITANIUM DIOXIDE: THEORY AND COMPUTATIONS

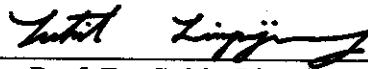
Suranaree University of Technology has approved this thesis submitted in partial fulfillment of the requirements for the Master's Degree.

Thesis Examining Committee



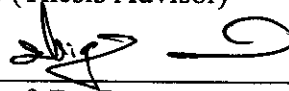
(Assoc. Prof. Dr. Prapun Manyum)

Chairperson



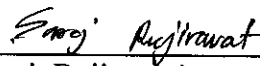
(Assoc. Prof. Dr. Sukit Limpijumnong)

Member (Thesis Advisor)



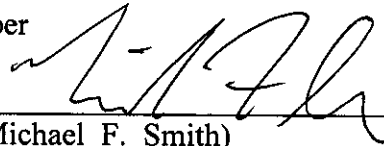
(Asst. Prof. Dr. Prayoon Songsiriritthigul)

Member



(Dr. Saroj Rujirawat)

Member



(Dr. Michael F. Smith)

Member



(Assoc. Prof. Dr. Saowanee Rattanaphani)



(Assoc. Prof. Dr. Sompong Thammathaworn)

Vice Rector for Academic Affairs

Dean of Institute of Science

สุทัศน์ ฌ พัทลุง : การศึกษาความบกพร่องในไทเทเนียมไดออกไซด์: เริงทฤษฎีและ
เชิงคำนวณ (DEFECTS IN TITANIUM DIOXIDE: THEORY AND
COMPUTATIONS) อาจารย์ที่ปรึกษา : รองศาสตราจารย์ ดร.ชูกิจ ลิมปิจำนงค์,
67 หน้า. ISBN 974-533-578-9

ไทเทเนียมไดออกไซด์เป็นหนึ่งในสารโพโตคะตะลิสต์ที่เป็นที่รู้จักกันเป็นอย่างดี โดยมี
โครงสร้างที่พบในธรรมชาติอยู่สามรูปแบบ คือ รูไทล์ อนาเทส และ บรูไคท์ ทั้งนี้ มีเฉพาะ
โครงสร้างแบบเตตระกอนอล คือ รูไทล์ และอนาเทส ที่เป็นที่พบเห็นโดยทั่วไป สำหรับไทเทเนียม
ไดออกไซด์ชนิดผงซึ่งถูกนำไปใช้เป็นสารโพโตคะตะลิสต์นั้น ส่วนมากมักจะมีโครงสร้างอนาเทส
ดังนั้นงานวิทยานิพนธ์นี้ จึงเน้นศึกษาโครงสร้างอนาเทส ผลการศึกษาคำนวณได้ค่าตัวแปรโครงร่าง
ผลึกอนาเทส ดังนี้ $a = 3.764$ อังสตรอม, $c/a = 2.515$, และ $u = 0.208$ ซึ่งมีค่าสอดคล้องเป็นอย่างดี
กับทั้งค่าที่วัดได้จากผลการทดลอง และ ค่าที่คำนวณได้โดยกลุ่มวิจัยอื่น ในวิทยานิพนธ์นี้ได้
ทำการศึกษาความบกพร่องมูลฐานของไทเทเนียมไดออกไซด์โดยอาศัยการคำนวณแบบเพิร์สพรีนซิ
เพิลซูโดโพเทนเชียลด้วยทฤษฎีฟังก์ชันแนลความหนาแน่น เท่าที่ทราบผลงานวิจัยนี้นับได้ว่าเป็นผล
การศึกษาคความบกพร่องชนิดมูลฐานในอนาเทสไทเทเนียมไดออกไซด์จากการคำนวณระดับเพิร์ส-
พรีนซิเพิลที่สมบูรณ์ที่สุดในปัจจุบัน ทั้งนี้เราพบว่าความบกพร่องมูลฐานอันได้แก่การที่มีอะตอม
แทรกหรือขาดนั้น มีค่าพลังงานก่อเกิดต่ำ ทำให้เป็นความบกพร่องชนิดที่น่าจะเกิดขึ้นจริง
โดยเฉพาะอย่างยิ่งไทเทเนียมที่แทรกมาในที่ว่างผลึก (Ti) ซึ่งเป็นตัวที่ให้อิเล็กตรอนได้สี่ตัวนั้น
มีค่าพลังงานก่อเกิดต่ำที่สุดในสารตัวอย่างชนิดพี ในขณะที่การขาดไทเทเนียม (V_{Ti}) ซึ่งเป็นตัวรับที่
รับอิเล็กตรอนได้สี่ตัว มีค่าพลังงานก่อเกิดต่ำที่สุดในสารตัวอย่างชนิดเอ็น ส่วนออกซิเจนที่แทรกมา
ในที่ว่างผลึก (O_i) พบว่าไม่เสถียรและจะเข้าไปจับกับออกซิเจนในแลตทิซ กลายเป็นออกซิเจน
โมเลกุล ที่มีประจุศูนย์ แทนที่ในตำแหน่งของออกซิเจน ทั้งนี้ สิ่งน่าสนใจเป็นอย่างยิ่ง คือผลการ
คำนวณแสดงให้เห็นว่าความบกพร่องมูลฐานทั้งสี่ชนิด (Ti, O_i , V_{Ti} , และ V_O) ไม่ทำให้เกิดระดับ
พลังงานของความบกพร่อง (defect levels) ขึ้นในช่องว่างแถบพลังงานของไทเทเนียมไดออกไซด์

สาขาวิชาฟิสิกส์
ปีการศึกษา 2549

ลายมือชื่อนักศึกษา สุทัศน์ ฌ พัทลุง
ลายมือชื่ออาจารย์ที่ปรึกษา ชูกิจ ลิมปิจำนงค์

SUTASSANA NA PHATTALUNG : DEFECTS IN TITANIUM DIOXIDE:
THEORY AND COMPUTATIONS. THESIS ADVISOR : ASSOC. PROF.
SUKIT LIMPIJUMNONG, Ph.D. 67 PP. ISBN 974-533-578-9

TITANIUM DIOXIDE/NATIVE DEFECTS/PHOTOCATALYST

TiO₂ is one of the most well known photocatalysts. There are three natural polymorphs of TiO₂: rutile, anatase, and brookite. Only the tetragonal polymorphs, i.e. rutile and anatase, are commonly found. Most of TiO₂ powder used in photocatalyst application is found in anatase phase. In this thesis, we focus our attention on the anatase structure. Our calculated crystal parameters of bulk anatase TiO₂ are: $a = 3.764$ Angstrom, $c/a = 2.515$, and $u = 0.208$, which are in agreement with the experimental values and other theoretical calculations. In this thesis, native point defects in anatase TiO₂ are investigated using first-principles pseudopotential calculations based on density-functional theory. To our knowledge, our result is the most complete first principles calculations of native defects in anatase TiO₂ to date. We found that fundamental native defects, i.e. interstitials and vacancies, have low formation energies, hence are likely to form. In particular, titanium interstitial (Ti_i) is a quadruple donor with the lowest formation energy under p-type conditions, whereas Ti vacancy (V_{Ti}) is a quadruple acceptor with the lowest formation energy under n-type conditions. We also found that an isolated oxygen interstitial (O_i) is not stable and spontaneously moves to bond strongly with a lattice O, leading to a charge-neutral O₂ molecule substituting on an O site. Interestingly, our calculations show that all four fundamental native defects (Ti_i, O_i, V_{Ti} , and V_O) do not introduce any defect level inside TiO₂ band gap.

School of Physics

Academic Year 2006

Student's Signature Sutassana Na Phattalung

Advisor's Signature Sukit Limpijumnong

ACKNOWLEDGMENTS

I am grateful to my thesis advisor, Assoc. Prof. Dr. Sukit Limpijumnong, for his valuable advices, comments for my thesis, for kindness, and suggestions about positive thinking. I thank the thesis examining committee members for their efforts throughout the entire process. These include Assoc. Prof. Dr. Prapan Manyam, Dr. Saroj Rujirawat, Asst. Prof. Dr. Prayoon Songsiriritthigul, and Dr. Rungnapa Thongpool. I would like to thank international co-authors, Drs. K. Kim, M-H. Du, S.-H. Wei, and S.B. Zhang, at National Renewable Energy Laboratory (USA) who make valuable contribution to our manuscript on native defects in TiO_2 that we published in Physical Review B. I thank all professors at the School of Physics for their kind attitude and providing me valuable knowledge. I would like to pay special thanks to Dr. Michael F. Smith at National Synchrotron Research Center for his fruitful guidances, kind attentions, and participating as a thesis examining committee member.

There are many peoples who helped me: Pakpoom Reunchan, Kanoknan Sarasamak, Jiraroj T. Theinprasert, Adisak Boonchum, Sirichok Jungthawan, Karnchana Limboonsong, and Secksan Sukasena.

I thank all graduate students in School of Physics for their support, encouragement and made this a fun time.

I would like to thanks Development and Promotion of Science and technology Talents project (DPST), National Synchrotron Research Center, and The Thai Research Fund for financial support.

Last, but certainly not least, it is my pleasure to thank my beloved family for their support, believe, and encourage.

Sutassana Na Phattalung

CONTENTS

	Page
ABSTRACT IN THAI.....	I
ABSTRACT IN ENGLISH.....	II
ACKNOWLEDGEMENTS.....	III
CONTENTS.....	V
LIST OF TABLES.....	XIII
LIST OF FIGURES	IX
LIST OF ABBREVIATIONS.....	XII
CHAPTER	
I INTRODUCTION.....	1
II THEORETICAL APPROACH.....	5
2.1 Ab-initio Methods.....	5
2.1.1 Born-Oppenheimer Approximation.....	6
2.1.2 Density Functional Theory	6
2.1.2.1 Hohenberg-Kohn Theorems.....	7
2.1.2.2 Kohn-Sham Equation.....	8
2.1.2.3 Local Density Approximation	10
2.1.2.4 Generalized Gradient Approximation	11
2.1.3 The Plane Waves	12
2.1.4 Pseudopotentials.....	13
2.1.5 Brillouin Zone, <i>k</i> -points and Monkhorst-Pack Method.....	14

CONTENTS (Continued)

	Page
2.2 The VASP Codes.....	15
III STRUCTURAL AND ELECTRONIC PROPERTIES OF BULK	
TiO₂	17
3.1 Structural Properties.....	17
3.1.1 The Polymorphs of TiO ₂	18
3.1.2 Structural Relaxations.....	22
3.2 Electronic Properties.....	22
3.2.1 Band Structure.....	22
3.2.2 Density of States.....	25
IV NATIVE DEFECTS IN ANATASE TiO₂	27
4.1 Introduction.....	27
4.2 Specific Computational Method for Defects Calculations.....	29
4.3 Results and discussion.....	34
4.3.1 Formation Energies and Charge States of Native Defects....	34
4.3.2 Structure and Stability of Native Defects.....	39
(a) Titanium Interstitial.....	39
(b) Titanium Vacancy.....	40
(c) Oxygen Interstitial.....	41
(d) Oxygen Vacancy.....	42
4.4 Conclusion.....	43
REFERENCES	45

CONTENTS (Continued)

	Page
APPENDIX.....	54
CIRRICULUM VITAE.....	67

LIST OF TABLES

Table		Page
3.1	The calculated crystal parameters of anatase TiO ₂ obtained using LDA and GGA in comparison with experimental values.....	20
3.2	The calculated crystal parameters and bulk modulus (<i>B</i>) of anatase and rutile TiO ₂ in comparison with Muscat <i>et al</i> 's calculations.....	21
3.3	High symmetry points in the BZ of anatase TiO ₂	23
4.1	Formation energy of native defects in anatase TiO ₂ with the Fermi level at the VBM. The results are shown for both the 48- and 108-atom supercells. Both the Ti-rich ($\mu_{\text{Ti}} = -2.67$ eV, precipitated by Ti ₂ O ₃ ; $\mu_{\text{O}} = -3.79$ eV) and O-rich ($\mu_{\text{Ti}} = -10.25$ eV; $\mu_{\text{O}} = 0$ eV) conditions are shown.....	36

LIST OF FIGURES

Figure	Page
2.1 All-electron (solid lines) and pseudoelectron (dashed lines) potentials and their corresponding wave functions. r_c represents a radius at which all-electron and pseudopotential values match.....	13
3.1 Conventional primitive cells of anatase TiO ₂ . Large and small spheres represent titanium and oxygen atoms, respectively. The definition of the equatorial (d_{eq}) and apical (d_{ap}) bonds are labeled.....	18
3.2 Total energy of anatase TiO ₂ as a function of cell volume (left) and c/a (right). The optimized crystal parameters V_0 (or a_0) and c/a_0 are determined.	20
3.3 The Brillouin zone of anatase (body centered tetragonal bravias lattice with $c > a$). Black dots indicate high symmetry points. Blue arrows are reciprocal lattice vectors.....	24
3.4 LDA band structure of anatase TiO ₂	25
3.5 Site decomposed electron density of states (DOS). For each atom center, the local partial DOS in a sphere radius R (Ti: $R= 1.48 \text{ \AA}$, O: $R= 0.74 \text{ \AA}$) is calculated. The panels show (a) total DOS of anatase TiO ₂ , (b-c) site projected on Ti and O atoms, (d-g) spacial and orbital decomposition of DOS on Ti and O atoms. Vertical dash line indicates the position of the VBM.....	26

LIST OF FIGURES (Continued)

Figure	Page
<p>4.1 Graphic illustration of thermodynamic growth conditions for TiO_2, i.e. the allowed values of the atomic chemical potentials, μ_{Ti} and μ_{O}. The dot-dashed horizontal and vertical lines indicate the upper bounds determined by the natural phases of Ti and O, respectively. Equilibrium growth of TiO_2 takes place for μ_{Ti} and μ_{O} lying on the solid line, whereas equilibrium growth of Ti_2O_3 and TiO takes place for μ_{Ti} and μ_{O} lying in the dashed and dotted lines, respectively.....</p>	32
<p>4.2 Atomic structures of (a) bulk anatase TiO_2, (b) Ti_i^{4+}, (c) V_{Ti}^{4-}, (d) $(\text{O}_2)_\text{O}$, and (e) V_{O}^{2+} defects. The large purple spheres are the Ti, the small green spheres are the O. Relaxation directions of neighboring atoms are selectively indicated by the arrows. In some cases, ideal positions of the atoms before relaxation or removal are shown by dashed circles.....</p>	34
<p>4.3 Defect formation energies as a function of the Fermi level, under the Ti-rich (left panel) and O-rich (right panel) growth conditions, respectively. The slope of the line is an indication of the charge state of the defect. The Fermi energy, referenced to the top of valence band, is all the way to the experimental band gap. The vertical dotted line is the calculated bandgap at the special k-point.....</p>	37

LIST OF FIGURES (Continued)

Figure	Page
<p>4.4 Site decomposed electron density of states (DOS). For each atom center, the local partial DOS in a sphere radius R (Ti:$R = 1.48 \text{ \AA}$ and O:$R = 0.74 \text{ \AA}$) is calculated. (a) Bulk TiO_2 where solid line is the total DOS, dashed line is the DOS on Ti, and dotted line is the DOS on O. (b-e) Native defects where the shaded area is the DOS on the atoms directly related to the defect (scaled up by a factor given in the parenthesis for clarity) and the solid line is the DOS on the remaining atoms in the supercell. Vertical dash-dotted line indicates the position of the VBM.....</p>	38

LIST OF ABBREVIATIONS

TiO_2	Titanium dioxide
VB	Valence band
CB	Conduction band
NHE	Normal Hydrogen electrode
E_g	Band gap
DFT	Density functional theory
Ψ	Wave function
E	Energy
\bar{R}	Position of a nuclei
\vec{r}	Position of electrons
\hat{H}	Hamiltonian
\hat{T}	Kinetic energy operator
\hat{V}	Electron-electron interaction operator
\hat{W}	Electron-ion interaction operator
$T_{TF}[\rho]$	Thomas-Fermi kinetic energy functional
$E_{TF}[\rho]$	Thomas-Fermi energy functional
$\rho(\vec{r})$	Density
$\rho_0(\vec{r})$	Ground-state density
$F_{HK}[\rho]$	Hohenberg-Kohn functional

LIST OF ABBREVIATIONS (Continued)

$V_{eff}(\vec{r})$	Effective single-electron potential
$V_{ext}(\vec{r})$	External potential
$V_{xc}(\vec{r})$	Exchange-correlation potential
$E_{xc}[\rho(\vec{r})]$	Exchange-correlation functional
$\epsilon_{xc}(\vec{r};[\rho(\vec{r})])$	Exchange-correlation energy/particle at the point
	r
$\lambda_F(\vec{r})$	Local Fermi wavelength
$\epsilon_{xc}[\rho(\vec{r})]$	Exchange-correlation energy per particle of a uniform electron gas of density $\rho(\vec{r})$
ϵ_x	Exchange energy
ϵ_c	Correlation energy
r_s	Radius of sphere containing one electron
LDA	Local density approximation
GGA	Generalized gradient approximation
$E_{xc}^{LDA}[\rho(\vec{r})]$	Exchange-correlation energy functional for non- spin polarized LDA
$E_{xc}^{GGA}[\rho(\vec{r})]$	Exchange-correlation energy functional for non- spin polarized GGA

LIST OF ABBREVIATIONS (Continued)

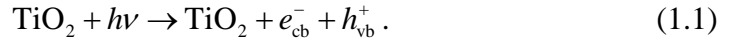
$f[\rho(\vec{r}), \vec{\nabla}\rho(\vec{r})]$	A function of both the electron density and the gradients of the density
PWs	Plane waves
$u_{i,\vec{k}}(\vec{r})$	Bloch function
$e^{i\vec{k}\cdot\vec{r}}$	Plane wave envelope
BZ	Brillouin zone
\vec{G}	Reciprocal lattice vector
E_{cut}	Kinetic energy cutoff
V	Volume of crystal
R_c	Cut-off radius
\vec{k}	Reciprocal lattice vectors with ends between the two k points
<i>et al.</i>	et alia (and other)

CHAPTER I

INTRODUCTION

TiO₂ is one of the most effective semiconductor photocatalysts (A semiconductor photocatalyst is typically a wide band gap semiconductor that, after being exposed to light, can increase the rate of certain chemical reactions without directly participating in these reactions.) It is widely used in various applications, for examples, deodorization, air purification, water treatment, and self-sterilization, all of which involve damaging microorganisms. The inactivation of Escherichia Coli, Coliform, and viruses have been reported (Ireland *et al.*, 1993; Watts *et al.*, 1995). Therefore, it is suitable for disinfecting waste water. The capability to damage microorganisms is partially a result of the high oxidizing power of TiO₂ valence band holes. Its (valence band hole) oxidizing power is comparable to that of SnO₂, WO₃ and ZnO. However, the chemical/photochemical stability of TiO₂ is very high in comparison with those materials (Barbeni *et al.*, 1985). Because TiO₂ is environmentally friendly, cheap, and powerful, it is of advantage over other semiconductor photocatalysts.

TiO₂, when photo-activated, can supply highly reactive holes that stimulate chemical reactions which lead to the disintegration of microorganisms. The process can be briefly described as follows. When TiO₂ is exposed to light with photon energy equal or larger than the band gap, an electron in the valence band (VB) jumps to the conduction band (CB), as described by the reaction (Ireland *et al.*, 1993):



The highly reactive hole in the VB can interact with water (H₂O) and/or hydroxyl (OH) adsorbed on the TiO₂ surface and produce hydroxyl radicals (OH[•]) (the solid circle superscript used in OH[•] and O₂^{•-} represents an electron lone pair) according to the reactions



and

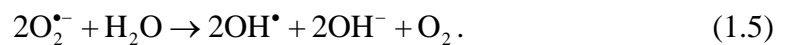


In order for the reaction in Eqs (1.2) and (1.3) to move forward, the VB edge of the catalyst (in this case TiO₂) has to be more positive than +1.23 V (the energy of the water splitting reaction in normal hydrogen electrode (NHE) scale (In the literature, redox potentials are usually given with respect to the normal hydrogen electrode (NHE) (Yong and Martin, 2000). Good semiconductor photocatalysts should have a low VB edge position or positive value (+1.23 V) in the NHE scale.). This emphasizes the importance of the low VB position of TiO₂.

In addition to holes, electrons excited to the CB can interact with oxygen molecules (O₂) on the surface, leading to superoxide ions (O₂^{•-}), described as



The resulting superoxide ions (O₂^{•-}) can further react with an adsorbed water, leading to hydroxyl radicals via



Thus both holes in the VB and electrons in the CB can, via different reactions, participate in surface reactions that eventually produce hydroxyl radicals. These

hydroxyl radicals are highly reactive and can rapidly attack organic compounds such as microorganisms. For example, a hydroxyl radical together with an oxygen molecule can decompose an organic compound $C_nO_mH_{(2n-2m+2)}$, into carbon dioxide molecules (CO_2) and water (H_2O) as described by



A good semiconductor photocatalyst for technological application should be (1) high photoactive; (2) chemically inert; (3) able to utilize visible and/or near-UV light; (4) cheap; and (5) photostable (Mill and Hunte, 1997).

The importance of the latter can be illustrated by the case of CdS. CdS is a small band gap semiconductor ($E_g=2.5$ eV) with a high conversion efficiency of visible light. However, CdS is unstable and photodegrades (Henglein, 1982), which makes it impractical in actual applications. In contrast to CdS, TiO_2 is a stable photocatalyst, but it has a large band gap of 3.0-3.2 eV (Mikami *et al.*, 2002). This band gap energy is in the UV range which means only a small fraction of sun light can be absorbed by TiO_2 . Although, this is a major problem in actual applications, it may be overcome by various methods of semiconductor modification, for e.g., metal-semiconductor modifications, use of composite semiconductors, surface sensitization and doping. Three directions to improve photocatalytic properties of semiconductor have been studied: (1) suppressing the electron-hole recombination by increasing the charge separation; (2) shifting the wavelength response range of semiconductor to visible light region; and (3) modifying the yield or selectivity of product (Linsebigler *et al.*, 1995).

The optimal band gap for high conversion efficiency of sun light spectra is ~ 2 eV (Bak *et al.*, 2002). However, TiO_2 has a larger band gap of 3.0-3.2 eV (Mikami *et*

al., 2002), making the activation of TiO_2 by sunlight ineffective. The UV light that can excite valence electrons of TiO_2 to the CB comprises only a small fraction (less than 5%) of the solar energy. Many research groups have tried to address this problem by modifying the TiO_2 band gap. Doping is the obvious way to do this. However, before one introduces the dopants, one should understand properties of native defects, which always exist in the background, so that the effects of dopants can be clearly distinguished.

This thesis is divided into four chapters. In chapter II, we give a brief overview of the theoretical approaches adopted. The purpose is to give the scope of our computational approach. We discuss additional computational parameters and details that are specific to certain parts of the work in chapters III and IV.

In chapter III, we report our study of bulk TiO_2 . The results include both structural and electronic properties. In the beginning of that chapter, we discuss the various polymorphs of TiO_2 and, in more detail, the structural relaxation of anatase phase. Later, electronic properties of the bulk material are shown.

In chapter IV, we present the main results of this thesis: the study of native defects in TiO_2 . The most likely fundamental native defects in anatase TiO_2 are theoretically identified and their properties are discussed.

CHAPTER II

THEORETICAL APPROACH

Theoretical schemes to calculate energy levels of electrons in a crystal have been developed extensively along with various approximations. The computational method used in this thesis is density functional theory (DFT) with local density approximation (LDA).

The aim of this chapter is to clarify the theoretical approach and some notations used in this thesis.

2.1 *Ab-initio* Method

Ab-initio or first principles methods are methods that do not need experimental parameters as inputs, other than the specification of the atomic elements in the system considered (i.e. the number of protons and electrons). The computations involve the approximation to the solution of the time-independent Schrödinger equation (Jiang, 2004)

$$\hat{H}\Psi(\vec{R},\vec{r})=E\Psi(\vec{R},\vec{r}). \quad (2.1)$$

To solve for electron arrangements, one needs to find the eigenstates, Ψ , and energies, E , that are solutions to Eq. (2.1). \vec{R} and \vec{r} represent the position of the nuclei and electrons, respectively. The Hamiltonian containing kinetic and potential terms can be written as (Eberlein, 2004)

$$\hat{H} = \hat{T}_n(\vec{R}) + \hat{T}_e(\vec{r}) + \hat{V}_{nn}(\vec{R}) + \hat{V}_{ee}(\vec{r}) + \hat{V}_{ne}(\vec{R}, \vec{r}) \quad (2.2)$$

This Hamiltonian is very complicated and, in practice, unsolvable. However, a number of useful approximations can simplify it.

2.1.1 Born-Oppenheimer Approximation

The Schrödinger equation of a crystal can be first simplified by separating the electron motion from the nuclear motion. Since the mass of an electron is much smaller than that of the nuclei, it can be assumed that the nuclei remain stationary as seen by an electron. Therefore, it is reasonable to separate the electronic motion from the nuclear motion. This assumption is known as the adiabatic approximation of Born and Oppenheimer or the Born-Oppenheimer approximation (Born and Oppenheimer, 1927).

However, even with Born-Oppenheimer approximation the Schrödinger equation is still enormously complicated. The simplest approach to this problem is to consider that a particular electron is only interacting with other electrons through the *electron density*, which has *3 degrees of freedom*, instead of the *electron wave functions*, which has *3N degrees of freedom*. This is essential to the approach known as density functional theory (DFT).

2.1.2 Density Functional Theory

The hypothesis that inspires the DFT development was introduced independently by Thomas (Thomas, 1927) and Fermi (Fermi, 1928). They assumed the existence of energy functional and proved that the kinetic energy can be written as a functional of the density of electrons $\rho(\vec{r})$ in an infinite potential well. The kinetic energy functional is given by

$$T_{TF}[\rho] = \frac{3}{10}(3\pi^2)^{2/3} \int d\vec{r} \rho^{5/3}(\vec{r}). \quad (2.3)$$

This equation is also the first introduction of a local density approximation (LDA). The Thomas-Fermi energy was given as

$$E_{TF}[\rho] = T_{TF}[\rho] - Z \int d\vec{r} \frac{\rho(\vec{r})}{|\vec{R} - \vec{r}|} + \frac{1}{2} \int d\vec{r}_1 d\vec{r}_2 \frac{\rho(\vec{r}_1)\rho(\vec{r}_2)}{|\vec{r}_1 - \vec{r}_2|}, \quad (2.4)$$

where Z is the nuclear charge. Since molecular bonding was not predicted in Thomas-Fermi theory, this theory cannot directly describe properties of bonds and many other flaws have been subsequently pointed out.

Density functional theory (DFT) is extensively used for quantum mechanically study of electrons in matters. It was developed in 1964-1965. Hohenberg-Kohn theorems (Hohenberg and Kohn, 1964) and Kohn-Sham equation (Kohn and Sham, 1965) are the core elements of DFT.

2.1.2.1 Hohenberg-Kohn Theorems

In 1964 Hohenberg and Kohn (henceforth, HK) investigated electron gas in a time-independent external potential (Hohenberg and Kohn, 1964) based on the foundation of the Thomas-Fermi theory. They developed two important theorems.

I). *The basic lemma of HK.* The ground-state density $\rho_0(\vec{r})$ of a bound system of interacting electrons in some external potential V_{ext} determines this potential uniquely.

II). The ground state energy is the variation minimum of the energy expression.

The total ground state energy is obtained from the variation principle by minimizing the energy with respect to the electron wave function. This can be written as

$$E_0 = E[\rho_0] = \langle \Psi[\rho_0] | \hat{T} + \hat{V} + \hat{W} | \Psi[\rho_0] \rangle \leq \langle \Psi[\rho] | \hat{T} + \hat{V} + \hat{W} | \Psi[\rho] \rangle = E[\rho], \quad (2.5)$$

if $\rho \neq \rho_0$

$$E_0 = \min_{\rho \in \mathcal{N}} E[\rho] = \min_{\rho \in \mathcal{N}} \left[\int dr \rho(\vec{r}) V_{ext}[\rho] + F_{HK}[\rho] \right], \quad (2.6)$$

where \hat{T} is the electron kinetic energy operator, \hat{V} is the electron-electron interaction operator, \hat{W} is the electron-ion interaction operator, and $F_{HK}[\rho]$ is a universal functional, valid for any number of particles and any external potential.

These theorems give a way to find the ground state electron density and ground state energy by minimizing the energy functional $E_0[\rho]$. However, there is no known explicit expression of the ground state energy functional $E_0[\rho]$.

These two Hohenberg-Kohn theorems reduce the problem of finding the ground state energy and density to a simple problem of three-dimension variational principles.

2.1.2.2 Kohn-Sham Equation

One year later, Kohn and Sham (Kohn and Sham, 1965) proposed a different approach to simplify DFT further by introducing a set of Kohn-Sham orbitals (orthonormal one-electron orbitals) of which the square equals the ground state electron density.

Then, they introduced an *exchange-correlation energy functional* describing the quantum interaction between electrons. The idea is to solve the problem of minimizing the ground state energy functional using a set of Schrödinger-like single-electron equations, known as Kohn-Sham equations.

In other words, they showed the simpler way to obtain the approximate values of the ground state energy and electron density of a many-electron system, that in principle can be found by directly solving the complicated set of multiple-electron Schrödinger equations. This simpler way can be done by computing the ground state energy of a set of independent electrons in an effective potential, where the sum of the single-electron ground state energies is assumed to be the actual ground state total energy. The self-consistent Kohn-Sham equations can be written as

$$\left[-\frac{\hbar^2 \nabla^2}{2m} + V_{eff}(\vec{r}) \right] \Psi_i(\vec{r}) = \varepsilon_i \Psi_i(\vec{r}), \quad (2.7)$$

where $V_{eff}(\vec{r})$ represents an effective single-electron potential, which is a functional of electron density. $V_{eff}(\vec{r})$ can be written as

$$V_{eff}(\vec{r}) = V_{ext}(\vec{r}) + \int d\vec{r}' \frac{\rho(\vec{r}')}{|\vec{r} - \vec{r}'|} + V_{xc}(\vec{r}), \quad (2.8)$$

where the exchange-correlation potential $V_{xc}(\vec{r})$ is determined by the derivative of the exchange-correlation functional $E_{xc}[\rho(\vec{r})]$ as

$$V_{xc}(\vec{r}) = \frac{\delta E_{xc}[\rho(\vec{r})]}{\delta \rho(\vec{r})}, \quad (2.9)$$

$$E_{xc}[\rho(\vec{r})] = \int d\vec{r} \varepsilon_{xc}(\vec{r}; [\rho(\vec{r})]) \rho(\vec{r}), \quad (2.10)$$

where $\varepsilon_{xc}(\vec{r}; [\rho(\vec{r})])$ is an exchange-correlation energy/particle at the point r , which is a functional of the density $\rho(\vec{r})$. It depends primarily on the density $\rho(\vec{r})$ at point \vec{r} near r , where “near” refers to a microscopic distance in the order of the local Fermi wavelength $\lambda_F(\vec{r}) \equiv [3\pi^2 \rho(\vec{r})]^{-1/3}$ or Thomas-Fermi screening length. Although, the

exact exchange-correlation energy functional in Eq. (2.10) is not known, a few standard approximations of it are introduced.

2.1.2.3 Local Density Approximation

The local density approximation (LDA) is the simplest and the most employed approximation to calculate exchange-correlation energy. In LDA, the exchange-correlation depends only on the *local* density. The exchange-correlation energy functional for non-spin polarized LDA can be written as

$$E_{xc}^{LDA}[\rho(\vec{r})] = \int dr \varepsilon_{xc}^{LDA}[\rho(\vec{r})]\rho(\vec{r}), \quad (2.11)$$

where $\varepsilon_{xc}[\rho(\vec{r})]$ is the exchange-correlation energy per particle of a uniform electron gas of density $\rho(\vec{r})$ (Kohn and Sham, 1965; Kohn, 1999). The exchange-correlation energy (ε_{xc}) is a sum between an exchange energy (ε_x) and a correlation energy (ε_c). The exchange part is given in atomic units by

$$\varepsilon_x^{LDA}(\rho) \equiv -\frac{0.458}{r_s}, \quad (2.12)$$

where r_s is the radius of sphere containing one electron and given by $\frac{4\pi}{3}r_s^3 = \rho(\vec{r})^{-1}$.

The correlation part is more complicated and was first estimated by Wigner (Wigner, 1938). It can be written as

$$\varepsilon_c^{LDA}(\rho) = -\frac{0.44}{r_s + 7.8}. \quad (2.13)$$

Since the exact $\varepsilon_c^{LDA}(\rho)$ is not known, obtaining the correlation energy E_c^{LDA} is not straightforward. In the beginning, perturbation theory was used to approximate the expressions $\varepsilon_c^{LDA}(\rho)$ (Barth and Hedin, 1972). Later, Cerperly, and Alder (1980)

calculated a more precise value of $\varepsilon_c^{LDA}(\rho)$ using Quantum Monte Carlo (QMC) calculations for electron liquid. Modern expressions for $\varepsilon_c^{LDA}(\rho)$ are obtained via parameterizations (Vosko *et al.*, 1980; Perdew *et al.*, 1981; Perdew *et al.*, 1993).

Theoretically, LDA should work well only for slowly varying densities system such as the weakly perturbed electron gas. However, it turns out to work surprisingly well even for inhomogeneous electron density systems such as the cases of atoms and molecules. LDA *ab-initio* lattice parameters are usually underestimated, while cohesive energies, elastic moduli, and phonon frequencies are usually overestimated.

2.1.2.4 Generalized Gradient Approximation

The generalized gradient approximation (GGA) (Perdew and Wang, 1986; Perdew *et al.*, 1996) was introduced to better treat systems with spacially varying or inhomogeneous density, found in real system. GGA allows the functional to depend also on gradient of the density in addition to density itself, making it more suitable for finite systems, such as atoms or molecules (Ortiz and Ballone, 1991). The usefulness of GGA in *periodic systems* has been controversial since it is unclear whether the additional computational resource used (in comparison to LDA) really leads to improved results (Filippi *et al.*, 1994; Khein *et al.*, 1995; Lee and Martin, 1997). The exchange-correlation energy functional for non-spin polarized GGA can be written as (Kohn, 1999)

$$E_{xc}^{GGA}[\rho(\vec{r})] = \int d\vec{r} f[\rho(\vec{r}), |\vec{\nabla}\rho(\vec{r})|] \rho(\vec{r}), \quad (2.14)$$

where $f[\rho(\vec{r}), |\vec{\nabla}\rho(\vec{r})|]$ is a function of both the electron density and the gradients of the density. Various choices of function $f[\rho(\vec{r}), |\vec{\nabla}\rho(\vec{r})|]$ were developed for

different variant of GGA. The most popular GGA are PBE (denoting the functional introduced by Perdew, Burke and Ernzerhof (Perdew *et al.*, 1996) mostly used in solid state physics, and BLYP [denoting the combination of Becke's exchange functional (Beck, 1988) and correlation functional of Lee, Yang, and Parr (Lee *et al.*, 1998)] mostly used in chemistry.

2.1.3 Plane Waves

Plane waves (PWs) are mathematically uncomplicated to use as a basis for describing electronic wave functions of periodic systems. Obvious advantages (in addition to the fact that PWs by themselves are solutions to zero-potential Schrödinger equations) include a good description of delocalized states, orthogonality and simple control of convergence (by varying the energy cutoff). Bloch's theorem stated that, in a periodic system, each electronic wave function can be written as a product of a periodic function or Bloch function $u_{n,\vec{k}}(\vec{r})$ and a plane wave envelope $e^{i\vec{k}\cdot\vec{r}}$. It can be written as (Payne *et al.*, 1992)

$$\Psi_{n,\vec{k}}(\vec{r}) = e^{i\vec{k}\cdot\vec{r}} u_{n,\vec{k}}(\vec{r}), \quad (2.15)$$

where

$$u_{n,\vec{k}}(\vec{r} + \vec{R}) = u_{n,\vec{k}}(\vec{r}). \quad (2.16)$$

PWs are also defined in terms of given reciprocal vector within the first Brillouin zone \vec{k} and reciprocal lattice vector \vec{G} ,

$$|\vec{k} + \vec{G}\rangle = \frac{1}{V} e^{i(\vec{k} + \vec{G})\cdot\vec{r}}, \quad \frac{\hbar^2}{2m} |\vec{k} + \vec{G}|^2 \leq E_{cut}, \quad (2.17)$$

where V is the volume of crystal and E_{cut} is the kinetic energy cutoff. PWs have various advantages, but are not suitable to describe a very localized nature of the charge density such as fast-oscillating wave functions near a nucleus.

2.1.4 Pseudopotentials

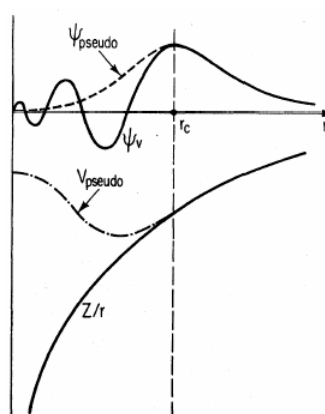


Figure 2.1 All-electron (solid lines) potential and pseudopotential (dashed lines) and their corresponding wave functions. r_c represents a radius outside which all-electron and pseudopotential values match (Payne *et al.*, 1992).

In the previous section, we have seen that PWs basis set provides a (mathematically) simple representation of a wave function. A drawback is that the PWs with a limited E_{cut} can not well describe core states. It is computationally impractical to represent the strong-oscillation wavefunctions in the core region with a PWs basis set with a very high energy cutoff (Heine, 1970). Elements below helium on the periodic table have fully filled inner shells of electrons which are strongly bound to the nucleus. It is often assumed that one can treat the core electrons within the frozen core approximation, which assumes the core electrons to be insensitive to chemical bonding characterized by the valence electrons. In this view, it is a good

approximation to treat the combination of the core electrons and nucleus as an hypothetical external potential (called pseudopotentials) acting on the valence electrons. The pseudopotential can be separated into two regions (Stibor, 2001).

I). The *core-region* defined within the cut-off radius R_c , is the region where in reality the electrons are in the direct vicinity of the core. The neighboring atoms do not noticeably influence the tightly bound core-electrons which are confined in this region. The actual electrons wave functions oscillate rapidly in this region and the actual potential is strongly attractive.

II). The *interatomic-region* is the home to valence electrons which is responsible for the interatomic binding. The valence electrons wave functions and potential in this region oscillate slowly.

The pseudopotential concept is to eliminate the nodal structures of the valence electron wave functions, making the PWs expansion of the wave functions converges faster, by replacing the strong electron-ion potential with a pseudopotential with the strongly negative core region removed. Figure 2.1 shows a comparison between the pseudopotential and the actual potential. This change in the core region only effects the electron wave functions within the core region and kept the wave function in the interatomic-region intact.

2.1.5 Brillouin Zone, k -points and the Monkhorst-Pack method

Under DFT, a complicated many body problem of electrons in a material is reduced to individual non-interacting single electron problems in an effective potentials. However, it is still impossible to solve an infinite body problem of non-interacting electrons moving in potential from an infinite number of ions. The problem, however, can be vastly simplified by taking advantage of the periodicity of

the system through the periodic boundary conditions (PBC). In this view, the Bloch theorem (Bloch, 1928) states that every k -point outside of the first Brillouin zone (BZ) relates to the k -point inside the first BZ through the linear combination of reciprocal lattice vectors and the eigenstate vary from the k -point outside the first BZ to the corresponding k -point inside the first BZ by a phase factor $e^{i\vec{k}\cdot\vec{r}}$ where \vec{k} is the reciprocal lattice vectors with ends between the two k points. Therefore, the total energy per (real space) unit cell of an infinite crystal can be calculated by integrating the energies of all occupied eigenstates within the first BZ. To do this, one needs to solve Kohn-Sham equations of as many k points inside the first BZ as possible. However, there are approximately 10^{23} possible k points inside the first BZ. To solve Kohn-Sham equation using all k points is, hence, impossible. In reality, the integral of the eigen energies converges as a function of k points rather quickly. Therefore, only a sampling set of k points is actually needed. Monkhorst and Pack (1976) introduced a special way to choose the set of sampling k -pints within the first BZ that works exceptionally well and have been widely used.

2.2 The VASP Codes

The Vienna Ab Initio Simulation Package (VASP) (Kresse and Furthmüller, 1996; Kresse and Hafner, 1993; Kresse and Hafner, 1994) is a pseudopotential-based program that employed DFT and periodic boundary conditions. It uses a plane wave basis set to describe electron wave functions. In this work, a special type of pseudopotential called ultrasoft pseudopotentials (Vanderbilt, 1990; Kresse and Hafner, 1994), which allows low energy cutoff for PWs basis set, are used. We use the Ceperley and Alder method (Ceperley and Alder, 1980) with the correlation described

by the Perdew and Zunger (Perdew and Zunger, 1981) in the exchange-correlation energy calculations. The k -point sampling is based on the Monkhorst-Pack approach (Monkhorst and Pack, 1976). The lattice parameters and atomic positions are allowed to relax using a conjugate gradient scheme. The Methfessel and Paxton method (Methfessel and Paxton, 1989) is used to treat partial band occupancy of electrons.

VASP calculations consist of two main loops. First, in the inner loop, the Kohn-Sham equations are solved by a self-consistent algorithm. The total energy and the force matrix on each nucleus are determined. Second, in the outer loop, the optimization of the atomic positions (until the residue forces fall below the level set) are performed.

CHAPTER III

STRUCTURAL AND ELECTRONIC PROPERTIES OF BULK TiO₂

3.1 Structural Properties

3.1.1 The polymorphs of TiO₂

There are three natural polymorphs of TiO₂: rutile ($P4_2/mnm$), anatase ($I4_1/amd$) and brookite ($Pbca$). Out of these three phases, only the tetragonal phases (rutile and anatase) are commonly found. TiO₂ is a wide band-gap semiconductor with a band gap of 3.03 eV for rutile and 3.18 eV for anatase (Asahi *et al.*, 2001). In the past, theoretical works predicted that rutile is more stable than anatase (Park *et al.*, 2002; Mo and Ching, 1995). However, recently Muscat *et al.* (2002) predict anatase to be slightly more stable than rutile. Both phases of TiO₂ have various applications: solar cells, lithium batteries, optical coating, and photocatalysis, to name a few. The Fermi level of anatase is higher than rutile by about 0.1 eV (Mo and Ching, 1995), making the conversion efficiency of anatase-TiO₂ slightly higher than rutile-TiO₂. The anatase-TiO₂ thin film has a smaller electron effective mass and a larger optical absorption gap than the rutile-TiO₂. Since we are interested in TiO₂ power, which exists primarily in anatase phase, we focus our attention on anatase TiO₂.

Anatase has the body centered tetragonal structure. The conventional primitive cell contains six atoms. The represented conventional cell contains two unit cells (12 atoms) and is shown in Figure 3.1.

To describe the tetragonal Bravais lattice, two crystal parameters a and c/a are used.

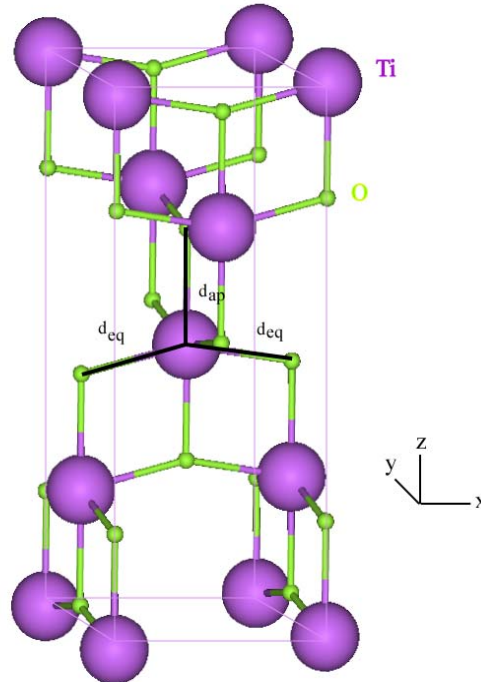


Figure 3.1 Conventional primitive cells of anatase TiO_2 . Large and small spheres represent titanium and oxygen atoms, respectively. The equatorial (d_{eq}) and apical (d_{ap}) bonds are labeled

3.1.2 Structural Relaxations

The atomic and electronic structures of TiO_2 are studied using first-principles calculations. This type of calculations is parameter-free and produces reliable results from fundamental quantum mechanics. We use the plane-wave, (ultrasoft) pseudopotential calculations (Vanderbilt, 1990; Kresse and Hafner, 1994) and density functional theory (Hohenberg and Kohn, 1964; Kohn, 1999; Kohn and Sham, 1965) as implemented in the Vienna *Ab-initio* Simulation Package (VASP) codes (Kresse and

Furthmüller, 1996; Kresse and Hafner, 1993; Kresse and Hafner, 1994). This approach

is known to be reliable in reproducing various properties such as microscopic arrangements, bulk modulus, phonon frequency, electron and hole effective masses, and electron density. We use the cutoff energy for the plane wave basis of 300 eV.

The structural optimization procedure involves the optimization of two external crystal parameters, a and c/a (the internal lattice parameter, which describes the length of the Ti-O bond, is optimized for each $a, c/a$). We would like to find a set of a and c/a that gives the lowest total energy. The most direct way, though not computationally efficient, is by calculating several pairs of a and c/a with a small grid spacing around the experimental values and search for the minimum point in this two-dimensional parameter space. (For each calculation, all atoms in the unit cell are allowed to relax.) To search for the minimum point in a and c/a coordinates at less computational cost, we choose to optimize each parameter one at a time, iteratively, according to the following scheme.

- 1) Volume (or a) optimization: Begin with the experimental values of c/a , a and atomic positions, we calculate total energy as a function of unit cell volume (V) with fixed c/a , and obtain the minimum volume (V_0) by cubic fit. (If the range investigated is sufficiently small, the Energy-Volume curve can be fit well using only a parabola.)
- 2) c/a optimization: From the optimized volume and (calculated) atomic positions, we calculate the energy as a function of c/a with the volume fixed. The cubic equation is, again, used to fit the Energy- c/a curve and find the optimum c/a . If new c/a is significantly varied from the initial value, step 1) is repeated.

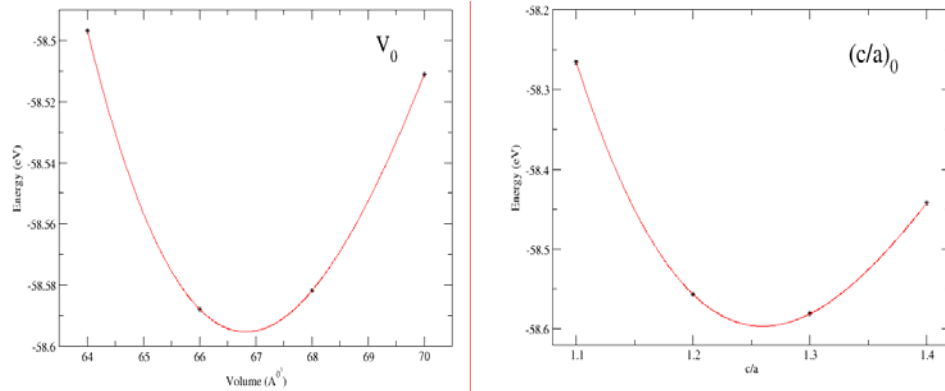


Figure 3.2 Total energy of anatase TiO_2 as a function of cell volume (left) and c/a (right). The optimized crystal parameters V_0 (or a_0) and c/a_0 are determined.

Table 3.1 The calculated crystal parameters of anatase TiO_2 obtained using LDA and GGA in comparison with experimental values [various sources, taken from Ref. (Burdett *et al.*, 1987)].

Parameter	Present		Exp. ^a
	LDA	GGA	
a (Å)	3.76	3.81	3.78
c (Å)	9.48	9.76	9.50
c/a	2.52	2.56	2.51
d_{eq} (Å)	1.92	-	1.93
d_{ap} (Å)	1.97	-	1.98
V_0 (Å ³ /molecule)	33.41	35.25	33.98

^a (Burdett *et al.*, 1987)

Table 3.2 The calculated crystal parameters and bulk modulus (B) of anatase and rutile TiO_2 in comparison with Muscat *et al.*'s calculations (Muscat *et al.*, 2002).

Parameter	Anatase		Rutile	
	Present	Theory ^b	Present	Theory ^b
a (Å)	3.76	3.76	4.63	4.57
c (Å)	9.48	9.50	2.90	2.93
c/a	2.52	2.53	0.63	0.64
B (GPa)	199	194	247	243

^b(Muscat *et al.*, 2002)

Table 3.1 shows the comparison between our calculated crystal parameters with the experimental values. Both LDA and GGA produce the results in good agreement with the measured values, with the LDA being slightly better. Therefore, we use LDA for further calculations. Table 3.2 shows our calculated crystal parameters and bulk modulus of anatase- TiO_2 and rutile- TiO_2 in comparison with recent calculations by Muscat *et al.* (2002). Our results and Ref. (Muscat *et al.*, 2002) agree to within 3%. Our calculated crystal parameters of bulk anatase TiO_2 of $a = 3.764 \text{ \AA}$, $c/a = 2.515$, and $u = 0.208$ are in good agreement with the experimental values of $a = 3.785 \text{ \AA}$, $c/a = 2.513$, and $u = 0.208$ (Burdett *et al.*, 1987). These values are also in good agreement with other calculations (Fahmi *et al.*, 1993; Asahi *et al.*, 2000; Calatayud *et al.*, 2001).

3.2 Electronic Properties

TiO₂ is often viewed as a strong ionic material with Ti⁴⁺ as the cation and O²⁻ as the anion. However, it also has some covalent characteristics (Zhang *et al.*, 1991; Nerlov *et al.*, 1996). The Ti atom (with a high oxidation number of +4) has six O (oxidation number -2) nearest neighbors and only 4 Ti next-nearest neighbors. The actual charge transfer between Ti and O by Bader analysis is actually smaller than the oxidation number, i.e. $Q_{\text{Ti}} = 2.96e$ and $Q_{\text{O}} = -1.48e$ (Calatayud *et al.*, 2001). Disregarding a small difference between the equatorial and apical neighboring bond distances, each Ti atom has six O neighbors and each O atom has three Ti neighbors.

Since the TiO₂ system is essentially ionic, it is quite different from other traditional semiconductors. For example, the electron counting and bonding orbital picture typically work well for tetrahedrally bonded semiconductors, does not work out for TiO₂.

3.1.1 Band Structures

Band structures are one of the fundamental electronic properties of crystalline material. Following the standard practice in presenting electronic band structures, band structures along selected lines between high symmetry k points in the first BZ are shown. The high symmetry points are shown in Table 3.3

Primitive vectors

$$\vec{a}_1 = a\vec{x}$$

$$\vec{a}_2 = a\vec{y}$$

$$\vec{a}_3 = \frac{a}{2}\left(\vec{x} + \vec{y} + \frac{c}{a}\vec{z}\right)$$

Reciprocal vectors

$$\vec{b}_1 = 2\pi\left(\frac{\vec{x}}{a} - \frac{\vec{z}}{c}\right)$$

$$\vec{b}_2 = 2\pi\left(\frac{\vec{y}}{a} - \frac{\vec{z}}{c}\right)$$

$$\vec{b}_3 = 2\pi\left(\frac{2}{c}\vec{z}\right)$$

Table 3.3 High symmetry points in the BZ of anatase TiO₂.

Symmetry points	Cartesian coordinate $\left(\frac{2\pi}{a}\right)$
Γ	(0,0,0)
Z	$\left(0,0,\frac{a}{c}\right)$
X	$\left(\frac{1}{2},\frac{1}{2},0\right)$
P	$\left(\frac{1}{2},\frac{1}{2},\frac{a}{2c}\right)$
N	$\left(\frac{1}{2},0,\frac{a}{2c}\right)$

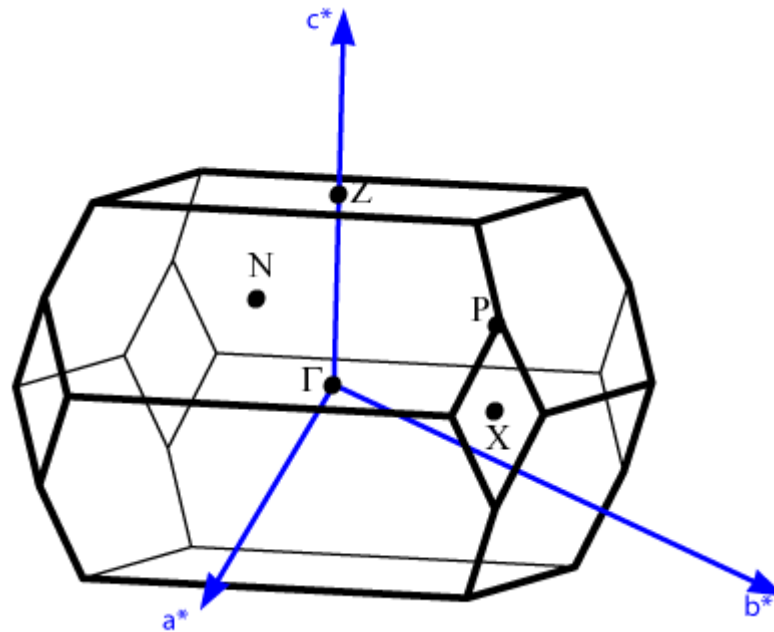


Figure 3.3 The Brillouin zone of anatase (body centered tetragonal bravias lattice with $c > a$). Black dots indicate high symmetry points. Blue arrows are reciprocal lattice vectors.

The electronic band structure of anatase TiO_2 are calculated using the unit cell containing 6 atoms. The calculated atomic coordinates and cell shape are used.

We found the bandgap to be indirect with the value of 1.87 eV. The bottom of the conduction band is located at Γ while the top of the valence band (VBM) is located at position $\Delta = (0.44, 0.44, 0)$ on the line between Γ and X.

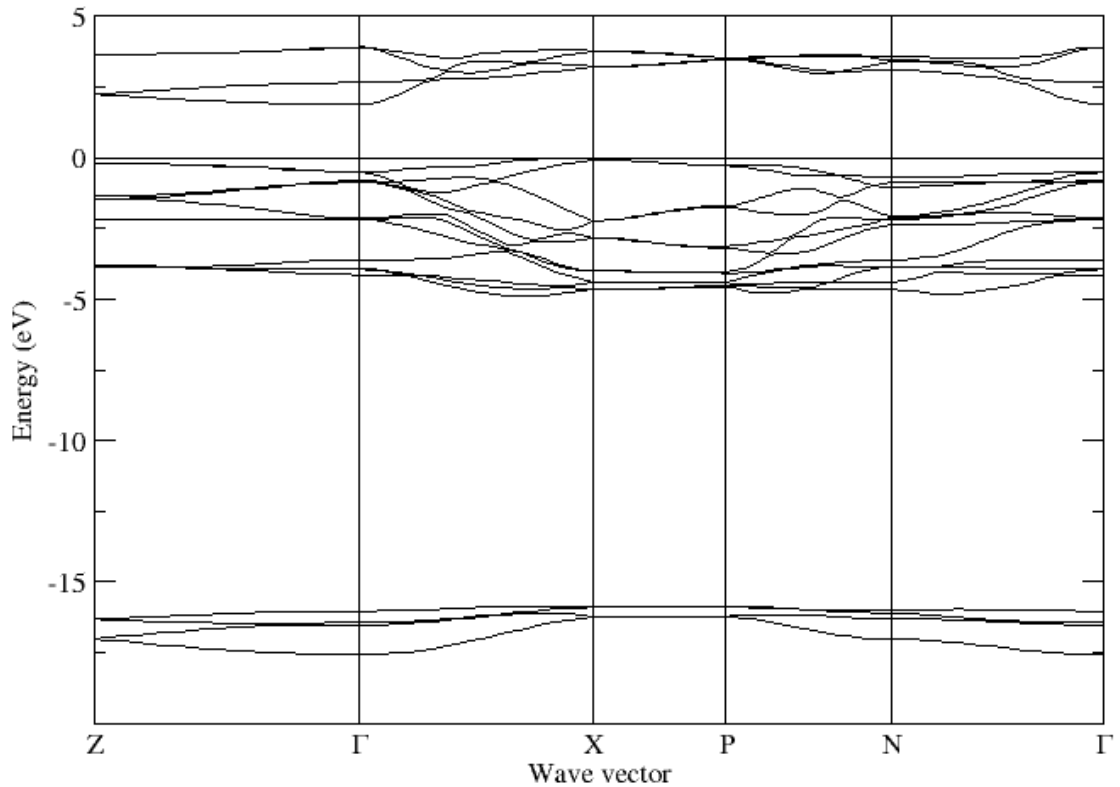


Figure 3.4 LDA band structure of anatase TiO₂.

3.1.2 Density of States

One of the most direct ways to understand the electronic nature of crystalline materials is by looking at their electron density of states (DOS). This is especially true, if one can look at the spatial and orbital decompositions DOS so that insight into the characteristics of each band can be obtained. For spatial decompositions, we calculated the local partial DOS in a sphere radius R (Ti: $R = 1.476 \text{ \AA}$ and O: $R = 0.741 \text{ \AA}$) centering on each nucleus. The DOS of bulk anatase TiO₂ is illustrated in figure 3.4.

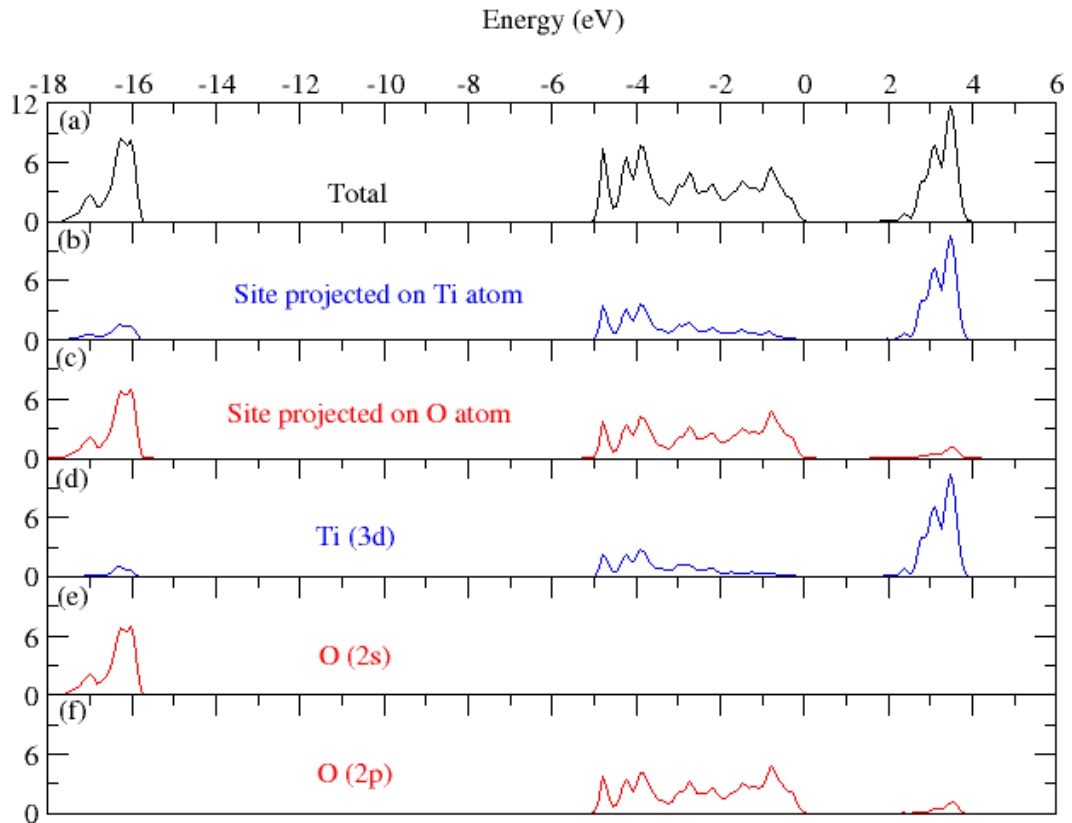


Figure 3.5 Site decomposed electron density of states (DOS). For each atom center, the local partial DOS in a sphere radius R (Ti: $R = 1.48 \text{ \AA}$, O: $R = 0.74 \text{ \AA}$) is calculated. The panels show (a) total DOS of anatase TiO_2 , (b-c) site projected on Ti and O atoms, (d-g) spacial and orbital decomposition of DOS on Ti and O atoms. Vertical dash line indicates the position of the VBM.

The bands at around 16 eV below VBM are composed mainly of the semi-core O $2s$. The valence bands (VB) are the mixture of O $2p$ and Ti $3d$: with the width of ~ 5.2 eV. The conduction bands (CB) near the band edge are mainly Ti $3d$ states.

The results of total DOS for bulk TiO_2 agree with those reported in other theoretical calculations (Asahi *et al.*, 2001; Calatayud *et al.*, 2001).

CHAPTER IV

NATIVE DEFECTS IN ANATASE-TiO₂

This chapter is the highlight of this thesis. The previous three chapters provided the background and computational details; it was demonstrated that we can reproduce basic properties of bulk TiO₂, using the described computational method, as accurately as has been henceforth reported in the literature. Having thus established some confidence in our computational scheme, we may move forward to study the complete fundamental native point defects in anatase TiO₂, which has not yet been done. A summary of this part of the work has been published in the Physical Review B journal (Na-Phattalung *et al.*, 2006).

4.1 Introduction

TiO₂ has been successfully applied as a semiconductor photocatalyst. Its main advantages over similar materials are its high oxidizing power and durability (i.e., high resistance to photo- and chemical corrosion). A major drawback of the TiO₂, however, is its large bandgap, which does not permit efficient absorption of visible light and hence prevents TiO₂ from being used in large-scale environmental applications. There is a rich literature describing the attempts to chemically dope TiO₂ in order to reduce the bandgap, but how to best manipulate the gap while maintaining the beneficial photocatalytic properties is still an unresolved challenge. For example, one of the difficulties in the chemical doping is that, while reducing the bandgap, the dopants

also act as carrier scattering centers and traps, which reduce the chance for the carriers to reach particle surfaces to participate in the desired reactions. Further complications arise in an effort to distinguish the effect of surface impurities from that of bulk impurities.

These problems underscore the need to understand, in detail, the changes in TiO_2 that result from impurity introduction. Before this can be done, however, one also has to understand the role of native defects in TiO_2 . Native defects could influence both of the factors mentioned above. The concentration of the native defects typically depends on the growth conditions, as well as on the presence of chemical impurities. This implies that it will be difficult for an experimentalist to unravel the effect of a particular chemical impurity simply from measuring the doping dependence of a photocatalytic process, because the native defects would likely also be playing some role. It is therefore desirable to study the properties of the native defects. At the very least, one should know what can be expected under the various growth conditions, so that the experimental results can be interpreted without any ambiguity arising from the contribution of the native defects.

Using first-principles total-energy calculations, we have investigated the fundamental native point defects in anatase TiO_2 . These include Ti vacancy (V_{Ti}), O vacancy (V_{O}), Ti interstitial (Ti_i), and O interstitial (O_i). All can have very low, and even negative, formation energies depending on the growth conditions. We have also studied the antisites and found that they have much higher energies due to the large cation-anion size mismatch and strong ionicity of TiO_2 . The formation energy of an antisite is even higher than the sum of those for vacancy and interstitial. For instance, the energy of O_{Ti} is higher than the sum of V_{Ti} and O_i . This means O_{Ti} is unstable

against spontaneous disintegration into a pair of isolated V_{Ti} and O_i . Hence, antisites are excluded from the discussion below. Due to a strong preference of the interstitial O_i to bind strongly with lattice O, however, substitutional diatomic molecule (O_2) always forms on the O site. To be consistent with our earlier work of defects in ZnO, we will call this paired oxygen $(O_2)_O$ (Limpijumnong *et al.*, 2005).

Interestingly, none of the above defects has a level inside the DFT bandgap. This finding is unexpected because, typically, native defects in wide gap semiconductors (Limpijumnong and Van de Walle, 2004; Neugebauer and Van de Walle, 1994; Limpijumnong *et al.*, 2004) do introduce deep levels inside the DFT gaps. Later in the article we will present a simple qualitative picture to show why the more ionic TiO_2 is distinct from other semiconductors in this way.

4.2 Specific Computational Method for Defects Calculations

We used the density functional theory (DFT) with the local density approximation (LDA) and ultrasoft pseudopotentials (Vanderbilt, 1990) as implemented in the VASP codes (Kresse and Furthmüller, 1996). The cutoff energy for the plane wave basis set is 300 eV. To calculate the formation energy of the defects, a supercell approach is used (Zhang and Northrup, 1991; Zhang, 2002) in which all atoms are allowed to relax by minimization of the Hellmann-Feynman force to less than 0.05 eV/Å. Our preliminary study was based on a supercell with 48 atoms, as a $2 \times 2 \times 2$ repetition of the primitive anatase unit cell. To ensure the convergence of the calculations, especially for high charge state defects, we repeated all the calculations with a larger supercell size of 108 atoms (namely, $3 \times 3 \times 2$). We found that formation energies calculated using the 48-atom cell typically agree to within 0.45 eV

with those calculated using the 108-atom cell (best case: $(\text{O}_2)_\text{O}^0$, 0.1 eV; worst case: V_Ti^{4-} , 0.76 eV). For the Brillouin zone integration, a $2 \times 2 \times 2$ Monkhorst-Pack special k-point mesh is used regardless of the cell size. Unless noted otherwise, all results presented here are based on the 108-atom cell calculations. We will present the electronic structure using a special k -point scheme as discussed in Ref. (Zhang, 2002). The calculated band gap averaged over the special k is 2.32 eV. Due to the well-known LDA gap error, the calculated band gap is smaller than the experimental band gap of 3.2 eV.

For a supercell, the defect formation energy is defined as (Zhang and Northrup, 1991)

$$E^f = E_{\text{tot}}(D^q) - E_{\text{tot}}(\text{TiO}_2, \text{bulk}) + \sum_x \Delta n_x \mu_x + qE_F, \quad (4.1)$$

where $E_{\text{tot}}(D^q)$ is the total energy of the cell with defect D in charge state q . $E_{\text{tot}}(0)$ is the total energy of the cell without the defect. Δn_X is the number of species X ($= \text{Ti}, \text{O}$) being removed from a defect-free cell, to its respective reservoir with chemical potential μ_X to form the defect cell. The chemical potential reflects the availability (or elemental partial pressure) of each element. During the growth, if any chemical potential rises above its natural phase value (i.e., that of hcp Ti and O_2 molecule), then the natural phase will form instead of the TiO_2 . Because of this, only the μ_X values below those of the natural phases need to be considered. More strict limitations on the chemical potentials may be further imposed by the formation of alternative phases containing both Ti and O, as will be discussed below.

If the TiO_2 crystal is to grow slowly, it is required that:

$$\mu_{\text{TiO}_2} = \mu_{\text{Ti}} + 2\mu_{\text{O}}, \quad (4.2)$$

where μ_{TiO_2} is the chemical potential of anatase TiO_2 . If we set $\mu_X = 0$ for their respective natural phases, then $\mu_{\text{TiO}_2} = -10.25$ eV is the calculated formation energy of anatase TiO_2 per molecular formula. The constraint, Eq. (4.3), ensures equilibrium growth conditions. If the sum on the right hand side is larger than μ_{TiO_2} , then the crystal will grow rapidly and will not be homogeneous. On the other hand, if this sum is lower than μ_{TiO_2} , then the crystal will disintegrate instead of grow.

In Figure 4.1, we illustrate the allowable conditions of growth on a graph of μ_{Ti} versus μ_{O} . The condition given by Eq. (4.3) is indicated by a solid line. There are other titanium-oxygen stable phases that may exist, including Ti_2O_3 and TiO . Since the Ti-to-O ratio is higher in both Ti_2O_3 and TiO than that in TiO_2 , we expect the growth of these alternate phases to be favorable under the Ti-rich growth conditions. To determine whether the formation of these alternative phases imposes a stricter upper limit on μ_{Ti} , we need to consider the equilibrium growth of Ti_2O_3 and TiO . For example for Ti_2O_3 , equilibrium growth takes place when

$$\mu_{\text{Ti}_2\text{O}_3} = 2\mu_{\text{Ti}} + 3\mu_{\text{O}}, \quad (4.3)$$

where $\mu_{\text{Ti}_2\text{O}_3} = -16.7$ eV is the calculated formation energy of Ti_2O_3 . Equation (4.3) (and the corresponding expression for TiO) is illustrated by a dashed (and dotted) line in Figure 4.1. We see that the lines corresponding to Eqs. (4.2) and (4.3) intersect at $\mu_{\text{Ti}} = -2.67$ eV. For higher values of μ_{Ti} , the growth of Ti_2O_3 is expected to proceed much more rapidly than that of TiO_2 , so that we may regard $\mu_{\text{Ti}} = -2.67$ eV as the real upper limit for the TiO_2 growth. With this, the range of allowable growth conditions is described by the bold solid line in Figure 4.1.

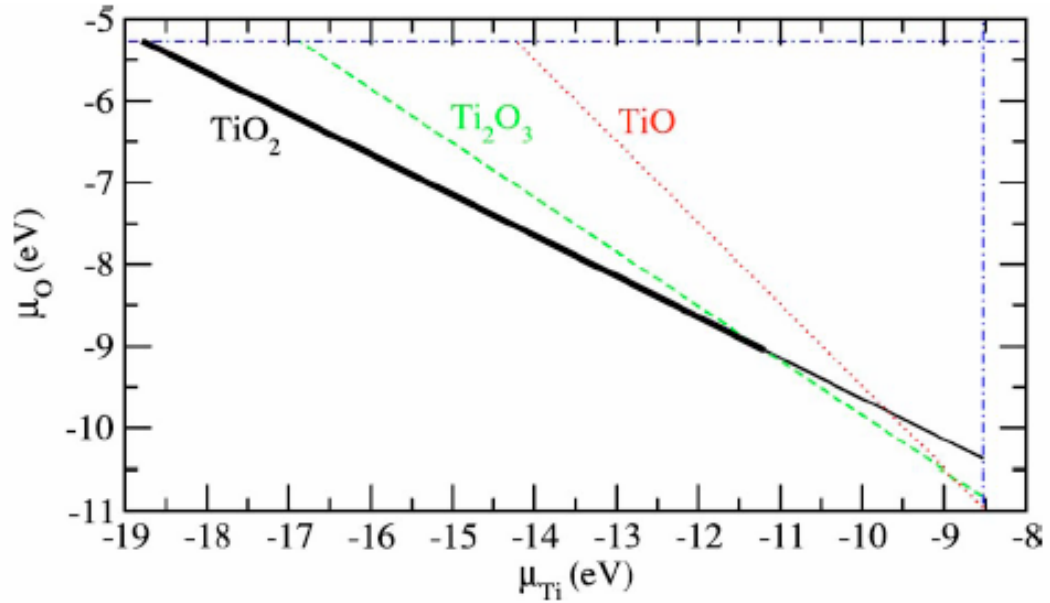


Figure 4.1 (Color online) Graphic illustration of thermodynamic growth conditions for TiO_2 , i.e. the allowed values of the atomic chemical potentials, μ_{Ti} and μ_{O} . The dot-dashed horizontal and vertical lines indicate the upper bounds determined by the natural phases of Ti and O, respectively. Equilibrium growth of TiO_2 takes place for μ_{Ti} and μ_{O} lying on the solid line, whereas equilibrium growth of Ti_2O_3 and TiO takes place for μ_{Ti} and μ_{O} lying in the dashed and dotted lines, respectively.

In our calculations, we vary the charge of the defect in order to identify the most stable charge state. To calculate the charged defects, a jellium background is used to neutralize the supercell. We have not applied any correction to the fictitious electrostatic interactions between the charged defect and its images in the neighboring supercells. This is justifiable especially in the case of TiO_2 where the dielectric constant ($\epsilon > 100$) (Parker, 1961) is about an order of magnitude higher than other semiconductors. The high dielectric constant results in small correction terms for the fictitious electrostatic interactions. For instance, the leading term of the Makov-Payne correction (Makov and Payne, 1995) for the charge state $4\pm$ in the 108-atom cell is

only about 0.1 eV, which is comparable to the expected error bars of our calculations. Moreover, we compare the results of the 48- and 108-atom cells to estimate the errors arising from the finite cell size and the supercell shape.

The concentration of a defect (c) is related to its formation energy E^f , through the equation

$$c = N_{\text{sites}} \exp(-E^f / kT), \quad (4.4)$$

where N_{sites} is the number of possible lattice sites per unit volume to form the defect, k is the Boltzmann's constant, and T is the temperature in Kelvin. To be exact, Eq. (4.6) is only valid under thermodynamic equilibrium. Actual growth of TiO_2 (as well as other semiconductors) is usually a non-equilibrium process. This means that the concentration of a defect can deviate substantially from that given by Eq. (4.6). Regardless of whether the growth/anneal process is under the thermal equilibrium or not, the formation energy is still a good indicator of the abundance of the defect: namely, defects with high formation energies are difficult to be incorporated and defects with lower formation energies are more likely to form.

Next section, we will plot formation energies as a function of E_F in order to consider the defect behaviors when doping level changes. This graph is a better presentation than defect concentration. Moreover, the dependence of formation energies on Fermi level shows the electrical activity (acceptor or donor) of a defect, the possible behavior of certain defect as compensation centers, and the position of its charge transfer.

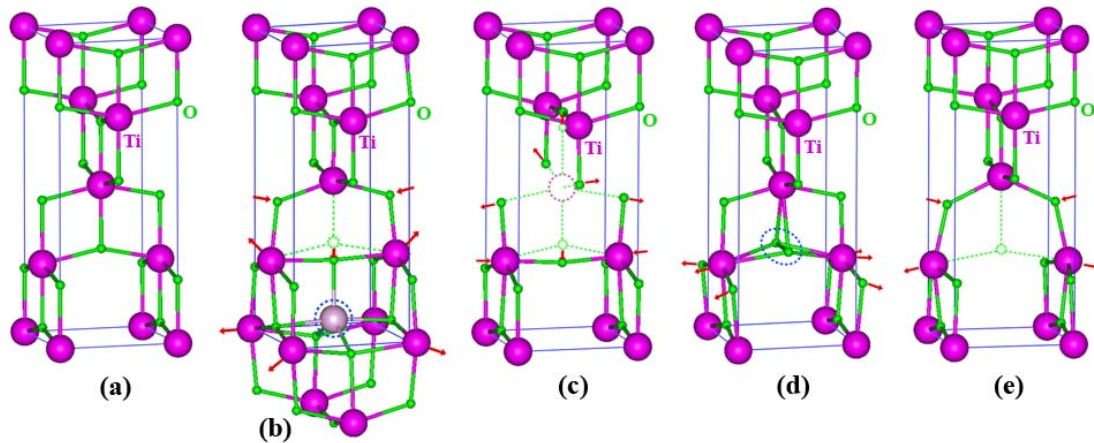


Figure 4.2 (Color online) Atomic structures of (a) bulk anatase TiO_2 , (b) Ti_i^{4+} , (c) V_{Ti}^{4-} , (d) $(\text{O}_2)_\text{O}$, and (e) V_O^{2+} defects. The large purple spheres are the Ti, the small green spheres are the O. Relaxation directions of neighboring atoms are selectively.

4.3 Results and Discussion

4.3.1 Formation Energies and Charge States of the Native Defects

Figure 4.2 shows the calculated atomic structures of Ti_i , V_{Ti} , $(\text{O}_2)_\text{O}$, and V_O . The defect formation energies are tabulated in Table I, as well as plotted as a function of the electron Fermi energy in Fig. 4.3. The most important feature of Figure 4.3 is that none of the defects introduce any defect levels inside the bandgap. The charge state of Ti_i , V_{Ti} , $(\text{O}_2)_\text{O}$, and V_O are $4+$, $4-$, 0 , and $2+$, respectively [The reported stable charge states of $+1$ and 0 for V_O are probably due to electron filling of the conduction band edge states rather than the actual defect states, because their calculated transition levels are > 2.6 eV above the VBM and are hence above our calculated CBM (They have used a very similar calculation method to ours)]. In contrast, native defects of semiconductors almost always introduce defect level in the bandgap (Van de Walle and Neugebauer, 2004; Kohan *et al.*, 2000) or near the band edges. Moving the Fermi level across the band gap cannot change the charge state of these defects. Even if the

Fermi level is moved into the valence or conduction band, there is still no significant filling of the defect, because the defect-induced electronic states are all delocalized resonant states, as revealed by the partial DOS in Figure 4.4 [For vacancies, the defect atoms include the nearest neighbors of the missing atom, i.e. six O atoms for V_{Ti} and three Ti atoms for V_{O} . For Ti_i , only the interstitial Ti atom itself is included as the defect atoms, whereas for $(\text{O}_2)_{\text{O}}$, both O atoms in the dimer are included]. As a result, none of these defects is a carrier trap. Due to the well-known LDA gap problems, our calculated conduction band minimum at the special k-points (ϵ_k) used for the Brillouin zone integration, indicated in Figure 4.3 by the dashed line, is smaller than the experimental gap. However, the defect states shown in Figure 4.4 are not expected to fall into the bandgap when a bandgap correction is applied, because they are all delocalized resonant states with symmetries resembling those of the extended band states (i.e., both the donors [Ti_i and V_{O}] and conduction band edge states have the Ti d character, while both the acceptors [$(\text{O}_2)_{\text{O}}$ and V_{Ti}] and valence band edge states have the O p character), which should follow the band edge closely in schemes that correct the LDA bandgap. In this regard, a GW quasiparticle calculation like the one in Ref. (Zhang *et al.*, 1989) is highly desirable to confirm such predictions.

Being free of native-defect-induced gap states is a result of high ionicity of the TiO_2 . The Ti has a small electronegativity (Ti = 1.54 in Pauling scale), smaller than the cations in all major group-IV, III-V, and II-V semiconductors, and the O has a very large electronegativity of 3.44. The defect states for Ti_i and V_{O} are the $\text{Ti}d$ states. Figure 4.4(b) and 4.4(e) show that these states are all above the CBM. In fact, a nominal Ti ion also has levels above the CBM.

Table 4.1 Formation energy of native defects in anatase TiO_2 with the Fermi level at the VBM. The results are shown for both the 48- and 108-atom supercells. Both the Ti-rich ($\mu_{\text{Ti}} = -2.67$ eV, precipitated by Ti_2O_3 ; $\mu_{\text{O}} = -3.79$ eV) and O-rich ($\mu_{\text{Ti}} = -10.25$ eV; $\mu_{\text{O}} = 0$ eV) conditions are shown.

Defect	Charge state	E_f (eV) (Ti-rich*)		E_f (eV) (O-rich)	
		48-atom	108-atom	48-atom	108-atom
Ti_i	+4	-9.88	-9.42	-2.32	-1.84
V_{Ti}	-4	12.64	13.40	5.06	5.82
$\text{O}_2 \equiv (\text{O}_2)_\text{O}$	0	4.50	4.40	0.71	0.61
V_{O}	+2	-2.82	-3.29	0.97	0.52
O_{Ti}	-4		21.91		10.54
Ti_{O}	+6		-6.83		4.53

*For Ti-rich case, we have taken into account the Ti_2O_3 , which has a lower energy than the Ti metal.

These explain why Ti_i and V_{O} do not induce gap levels, and, as a matter of fact, the large heat of formation of TiO_2 (-10.25 eV, see Section II). Also due to the high electron donating tendency of Ti, the O atoms around a V_{Ti} can easily draw electrons, resulting in defect states below the VBM.

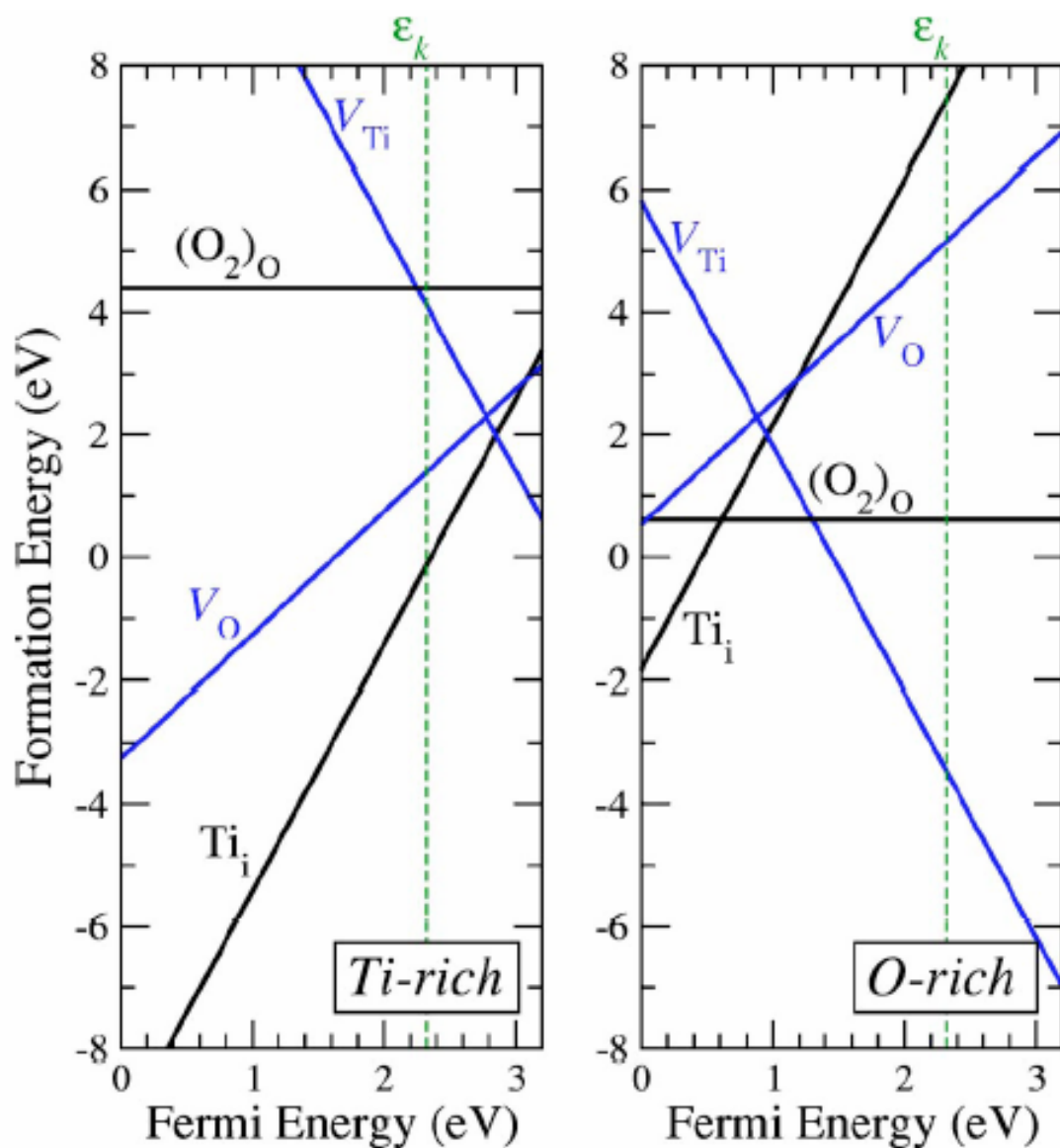


Figure 4.3 (Color online) Defect formation energies as a function of the Fermi level, under the Ti-rich (left panel) and O-rich (right panel) growth conditions, respectively. The slope of the line is an indication of the charge state of the defect. The Fermi energy, referenced to the top of valence band, is all the way to the experimental band gap. The vertical dotted line is the calculated bandgap at the special k -point.

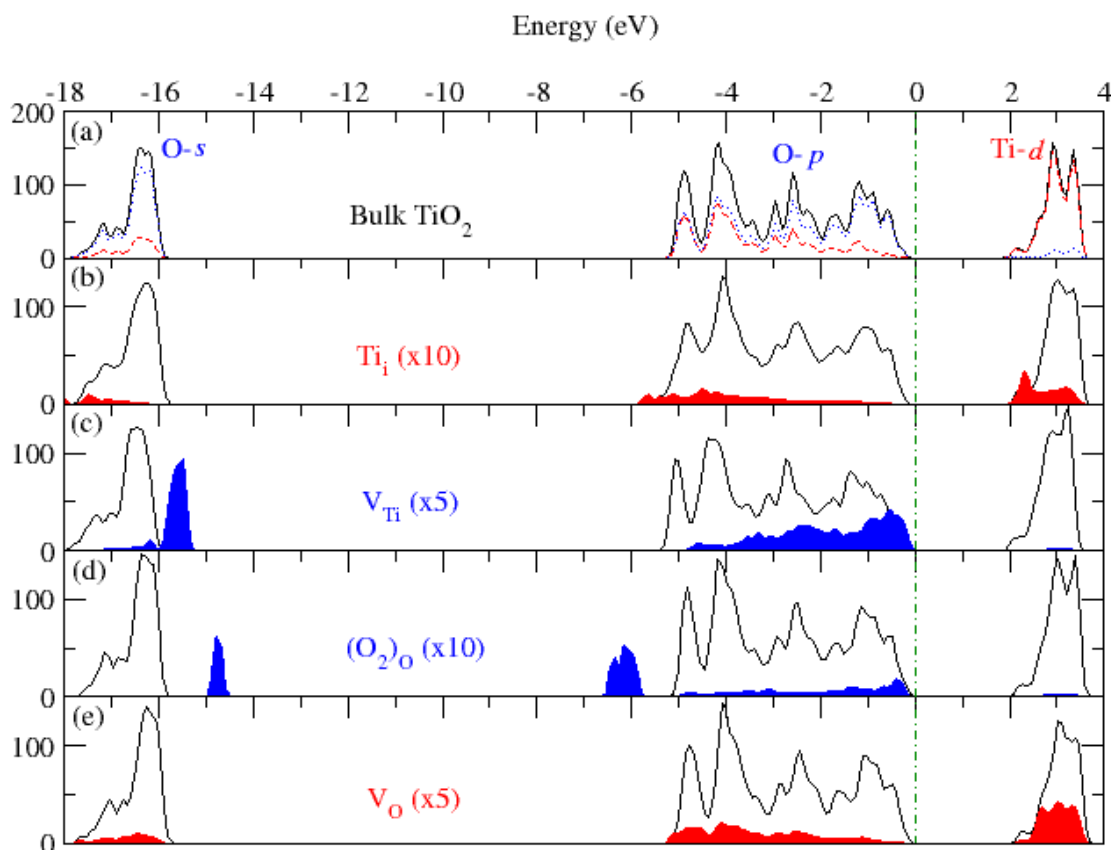


Figure 4.4 (Color online) Site decomposed electron density of states (DOS). For each atom center, the local partial DOS in a sphere radius R (Ti: $R = 1.48 \text{ \AA}$ and O: $R = 0.74 \text{ \AA}$) is calculated. (a) Bulk TiO_2 where solid line is the total DOS, dashed line is the DOS on Ti, and dotted line is the DOS on O. (b-e) Native defects where the shaded area is the DOS on the atoms directly related to the defect (scaled up by a factor given in the parenthesis for clarity) and the solid line is the DOS on the remaining atoms in the supercell. Vertical dash-dotted line indicates the position of the VBM.

4.3.2 Structure and Stability of the Native Defects

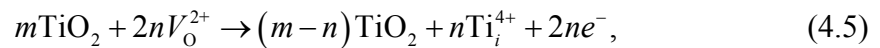
(a) Titanium interstitial (Ti_i)

Titanium interstitial favors an octahedral site [Figure 4.2(b)]. The site is similar to a lattice Ti site in that horizontally there are four neighboring O atoms near in a plane. The main difference is that the lattice Ti site also has two additional O atoms (one located directly above and one below). The *B* site places in the center of space and has five O neighbor atoms. The *B* site has four O neighbor atoms in diagonal axis (Ti-O distances of *B* site are longer than *A* site) and one O neighbor atom in vertical axis (located directly above). After relaxed the Ti_i in both *A* and *B* site will move to the same position [as shown in Figure 4.2(b)]. In the other words, after relaxed they are the same defect. One of the vertical O neighbors moves considerably towards it. The surrounding Ti atoms are also slightly relaxed outward, due to the electrostatic repulsion between positively charge Ti ions.

Ti_i is a *quadruple shallow donor*. Under the Ti-rich and *p*-type condition, i.e., E_F is at the VBM, which is the extremely favorable situation for Ti_i^{4+} incorporation, the formation energy of the Ti_i is negative and, surprisingly, very low, i.e. -9.42 eV. This low formation energy is due mainly to the energy gain from a transfer of four electrons to the low E_F level. In addition, the anatase structure contains a lot of open space that can accommodate the interstitial atom without much strain. [First principles studies of SnO_2 also found Sn_i^{4+} to have a negative formation energy at the cation-rich and *p*-type condition (Kiliç and Zunger, 2002).] This Ti_i formation energy remains to be negative as long as $E_F < 2.4$ eV (Figure 4.2, left panel). A negative formation energy means that the formation of the defect is spontaneous, so it is impossible to grow TiO_2 under such conditions. (Even if one begins in the *p*-type region, the rapid

formation of the quadruple donor Ti_i would quickly turn the sample n -type.) Under the O-rich condition, Ti_i may also have a negative formation energy unless $E_F > 0.5$ eV (see Figure 4.2, right panel). From these results, we expect it to be difficult to dope TiO_2 p -type under any equilibrium growth conditions.

The low formation energy of Ti_i makes it the strongest candidate for the shallow donors observed in undoped anatase TiO_2 with high purity (Forro *et al.*, 1994). The low formation energy may also explain the earlier observations of Ti_i in oxygen-deficient rutile samples by ion beam channeling (Yaki *et al.*, 1977), electron paramagnetic experiment (Aono and Hasiguti, 1993; Hasiguti and Yagi, 1994), and others as summarized in the review in Ref. (Sasaki *et al.*, 1985). Although most of the experimental works were performed on rutile TiO_2 , the local structures of rutile and anatase are very similar. Because the oxygen-deficient TiO_2 samples were prepared by heating TiO_2 (1000-1400 °C) in a reducing atmosphere for an prolonged period of time (typically 100-1000 hours), it is likely that some of the O atoms first migrate out of the sample; leaving vacancies behind. However, due to the small formation energy of Ti_i , these oxygen vacancies will subsequently react with remaining TiO_2 via the following reaction:



to produce Ti_i interstitials.

(b) Titanium vacancy (V_{Ti})

The atomic structure of V_{Ti} is shown in Figure 4.2(c) As one Ti atom is missing here, the surrounding O atoms relax outward; each to a point approximately halfway

between its two remaining Ti neighbors. This relaxation increases the Coulomb binding by reducing the Ti-O distances while increasing the O-O distances.

The Ti vacancy is a *quadruple shallow acceptor*. Under the O-rich (i.e. Ti-poor) growth condition, the formation energy of V_{Ti} is negative if $E_F > 1.46$ eV. This means that V_{Ti} will spontaneously form and, as a result (and because V_{Ti} is a quadruple acceptor), E_F will be pushed down until it is below 1.46 eV. Under the Ti-rich condition, V_{Ti} is still a low-energy defect, and hence, acts as a leading native acceptor. To the best of our knowledge, there is still no experimental identification of the V_{Ti} .

(c) Oxygen interstitial (O_i)

Isolated interstitial O has high formation energy and is hence unstable. It spontaneously binds with an O on the lattice site, forming a substitutional O_2 molecule, $(O_2)_O$. Each lattice O atom has an oxidation number of -2. A neutral $(O_2)_O$ thus contains two more electrons compared to a free O_2 molecule in the vacuum. Similar to the case of substitutional diatomic molecules in ZnO (Limpijumnong *et al.*, 2005), the additional two electrons occupy and completely fill the molecular $pp\pi^*$ states, which lie below the VBM. The atomic structure of the $(O_2)_O$ is shown in Figure 4.2(d). Because the charge neutral O_2 is electrostatically equivalent to any O atom on a lattice site, one can expect that there should not be any large relaxation of the neighboring atoms. All the neighboring Ti atoms relax only slightly outward. Substitutional O_2 has a bond length of 1.46 Å, which is very similar to substitutional O_2 in ZnO [also 1.46 Å (Limpijumnong *et al.*, 2005)]. The bond length of a substitutional O_2 is longer than that of a free O_2 [1.23 Å (Huber and Herzber, 1979)] due mainly to the occupation of the two extra electrons on the $pp\pi^*$ *antibonding*

orbital, and to the screening effect of the host. Under the Ti-rich condition, the $(\text{O}_2)_\text{O}$ has high formation energy and is hence unlikely to exist in any appreciable amount. However, under the O-rich condition, its formation energy is reasonably low, making it an important defect.

(d) Oxygen vacancy (V_O)

For O vacancy, each of the three nearest neighbor Ti atoms moves away from the vacancy toward its five remaining O neighbors, as illustrated in Figure 4.2(e). The next nearest neighbor O atoms move slightly inward due to the absence of electrostatic repulsion by the missing O atom.

Our calculations show that V_O is a *double donor*. This is because the O has an oxidation state 2- or, in other words, has two additional electrons transferred from the three surrounding Ti atoms. When the oxygen is removed as a neutral atom, the two additional electrons are no longer needed, making the V_O a double donor. This is consistent with first principles calculations by Sullivan and Erwin (2003). The formation energy of the V_O reported in Ref. (Sullivan and Erwin, 2003) is slightly higher than ours, partly because they used the “Makov-Payne correction” (Makov and Payne, 1995).

Our calculation suggests that V_O is *not* a dominant native defect *near equilibrium growth conditions*. Even in the Ti-rich growth condition, which is most favorable for V_O formation, Ti_i has a lower formation energy than V_O at all possible E_F . However, V_O can be created in certain processes such as the annealing to create oxygen-deficient samples. Although the energetics suggests that subsequent conversion to Ti_i via Eq. (4.5) is likely, the kinetics may not support such a process, as

one only needs to break the Coulomb bindings with three neighboring Ti to free an O, but six such bindings to free a Ti. This might be why V_O are still observed by certain experiments (thermogravimetric) electrochemical titration, diffusion, and conductivity measurements as discussed in Ref. (Sasaki *et al.*, 1985).

4.4 Conclusion

Our calculations of native defects in anatase TiO_2 provide detailed information on the atomic structures and electronic properties for each of them. We found that Ti_i is a quadruple donor with very low formation energy, especially in p -type samples but also in n -type samples. This makes it the strongest candidate responsible for the native n -type conductivity observed in TiO_2 . While V_O has higher formation energy than that of Ti_i , the kinetic barrier for creating V_O from a perfect TiO_2 is expected to be lower than that for creating Ti_i . Hence, post-growth formation of V_O is also possible, especially after the sample has been heated for a prolonged time. A quadruple acceptor V_{Ti} is the lowest energy acceptor in TiO_2 . Thus in undoped samples, Ti_i and V_{Ti} should be the leading donor and acceptor, respectively. Formation of Ti_i is further enhanced under the Ti-rich growth condition, while that of V_{Ti} is further enhanced under the O-rich growth condition. Interstitial oxygen would spontaneously bond to lattice oxygen, forming electrically inactive O_2 dimer substituting on one O lattice site. Antisite defects have relatively high formation energies and are likely to spontaneously break into isolated vacancies and interstitials. Our calculations also show that none of the four low-energy defects, Ti_i , O_i , V_{Ti} , and V_O , introduce any defect levels inside the DFT band gap.

REFERENCES

REFERENCES

- Aono, M. and Hasiguti, R. R. (1993). Interaction and ordering of lattice defects in oxygen-deficient rutile TiO_{2-x} . **Physical Review B** 48: 12406-12414.
- Asahi, R., Morikawa, T., Ohwaki, T., Aoki, K., and Taga, Y. (2001). Visible-Light Photocatalysis in Nitrogen-Doped Titanium Oxides. **Science** 13, 269-271.
- Asahi, R., Taga, Y., Mannstadt, W., and Freeman, A.J. (2000). Electronic and optical properties of anatase TiO_2 . **Physical Review B** 61: 7459-7465.
- Bak, T., Nowotny, J., Rekas, M., and Sorrell, C. C. (2002). Photo-electrochemical hydrogen generation from water using solar energy. **International Journal of Hydrogen Energy** 27: 991-1022.
- Barbeni, M., Pramauro, E., Pelizzetti, E., Borgarello, E., and Serpone, N. (1985). Photodegradation of pentachlorophenol catalyzed by semiconductor particles. **Chemosphere** 14: 195-208.
- Barth, U. von and Hedin, L. (1972). A local exchange-correlation potential for the spin polarized Case: I. **Journal of Physics: Condensed Matter** 5: 1629-1642.
- Becke, A. D. (1988). Density-functional exchange-energy approximation with correct asymptotic behavior. **Physical Review A** 38: 3098-3100.
- Bloch, F. (1928). **Zeitschrift fuer Physikalische** 52: 555.
- Born, M. and Oppenheimer, R. (1927). **Annals of Physics** 84: 457-484.
- Burdett, J. K., Hughbanks, T., Miller, G. J., Richardson, J. W., and Smith, J. V. (1987). **Journal of the American Chemical Society** 109: 3639-3646.

- Calatayud, M., Mori-Sánchez, P., Beltrán, A., Martín Pendás, A., Francisco, E., Andrés, J., and Recio, J.M. (2001). Quantum-mechanical analysis of the equation of state of anatase TiO₂. **Physical Review B** 64, 184113-184121.
- Ceperley, D. M. and Alder, B. J. (1980). Ground state of electron gas by a stochastic method. **Physical Review Letter** 45: 566-569.
- Eberlein, T. A. G. **Point and extended defects in group IV semiconductor** [Online].
Available: <http://newton.ex.ac.uk/research/qsystems/jones/thesis/eberlein-thesis.pdf>
- Fahmi, A., Minot, C., Silvi, B., and Causá, M. (1993). Theoretical analysis of the structures of titanium dioxide crystals. **Physical Review B** 47: 11717- 11724.
- Fermi, E. (1928). A statistical method for the determination of some atomic properties and the application of this method to the theory of the periodic system of elements. **Zeitschrift fuer Physikalische** 48: 73-79.
- Filippi, C., Singh, D. J., and Umrigar, C. J. (1994). All-electron local-density and generalized-gradient calculations of the structural properties of semiconductors. **Physical Review B** 50: 14947-14951.
- Forro, L., Chauvet, O., Emin, D., Zuppiroli, L., Berger, H., and Lévy, F. (1994). High mobility n-type charge carriers in large single crystals of anatase (TiO₂). **Journal of Applied Physics** 75: 633-635.
- Gunnarsson, O. and Lundqvist, B. I. (1976). Exchange and correlation in atoms, molecules, and solids by the spin-density-functional formalism. **Physical Review B** 13: 4274-4298.

- Hasiguti, R. R. and Yagi, E. (1994). Electrical conductivity below 3 K of slightly reduced oxygen-deficient rutile TiO_{2-x} . **Physical Review B** 49: 7251-7256.
- Heine, V. (1970). **The Pseudopotential Concept, vol. 24 of Solid State Physics** Academic Press: New York.
- Henglein, A. (1982). Photochemistry of colloidal cadmium sulfide. 2. Effects of adsorbed methyl viologen and of colloidal platinum. **Journal of Physical Chemistry** 86: 2291-2293.
- Hohenberg, P. and Kohn, W. (1964). Inhomogeneous electron gas. **Physical Review** 136: B864-B871.
- Huber, K. P. and Herzberg, G. (1979). **Molecular spectra and molecular structure. IV. Constants of diatomic molecules** New York: Van Nostrand Reinhold.
- Ireland, J. C., Klostermann, P., Rice, E. W., and Clark, R. M. (1993). Inactivation of *Escherichia coli* by titanium dioxide photocatalytic oxidation. **Applied and Environmental Microbiology** 59: 1668-1670.
- Jiang, C. **Theoretical studies of aluminium and aluminide alloys using calphad and first-principles approach** [On-line].
Available: http://etda.libraries.psu.edu/theses/approved/WorldWideFiles/ETD-579/PhD_Thesis.pdf
- Klein, A., Singh, D. J., and Umrigar, C. J. (1995). All-electron study of gradient corrections to the local-density functional in metallic systems. **Physical Review B** 51: 4105-4109.
- Kiliç, C. and Zunger, A. (2002). Origins of Coexistence of Conductivity and Transparency in SnO_2 . **Physical Review Letter** 88: 095501-095504.

- Kohan, A. F., Ceder, G., Morgan, D., and Van de Walle, C. G. (2000). First-principles study of native point defects in ZnO. **Physical Review B** 61: 15019 - 15027
- Kohn, W. (1999). Nobel lecture: electronic structure of matter-wave functions and density functionals. **Reviews of Modern Physics** 71: 1253-1266.
- Kohn, W. and Sham, L. J. (1965). Self-consistent equations including exchange and correlation effects. **Physical Review** 140: A1133-A1138.
- Kresse, G. and Furthmuller, J. (1996). Efficient iterative schemes for *ab initio* total-energy calculations using a plane-wave basis set. **Physical Review B** 54: 11169-11186.
- Kresse, G. and Furthmuller, J. (1996). Efficiency of *ab-initio* total energy calculations for metals and semiconductors using a plane-wave basis set. **Computational Materials Science** 6: 15-50.
- Kresse, G. and Hafner, J. (1993) Ab-initio molecular dynamics for liquid metals. **Physical Review B** 47:558-561.
- Kresse, G. and Hafner, J. (1994). Ab-initio molecular-dynamics simulation of the liquid-metal-amorphous-semiconductor transition in germanium. **Physical Review B** 49:14251-14269.
- Lee, C., Yang, W., and Parr, R. G. (1988). Development of the Colle-Salvetti correlation-energy formula into a functional of the electron density. **Physical Review B** 37: 785-789.
- Lee, I.-H. and Martin, R. M. (1997). Applications of the generalized-gradient approximation to atoms, clusters, and solids. **Physical Review B** 56: 7197-7205.

- Limpijumnong, S., Li, X., Wei, S.-H., and Zhang, S. B. (2005). Substitutional diatomic molecules NO, NC, CO, N₂, and O₂: Their vibrational frequencies and effects on *p* doping of ZnO. **Applied Physics Letter** 86: 211910-211913.
- Limpijumnong, S. and Van de Walle, C. G. (2004). Diffusivity of native defects in GaN. **Physical Review B** 69: 035207-035211.
- Limpijumnong, S., Zhang, S. B., Wei, S.-H., and Park, C. H., (2004). Doping by Large-Size-Mismatched Impurities: The Microscopic Origin of Arsenic- or Antimony-Doped *p*-Type Zinc Oxide. **Physical Review Letter** 92: 155504
- Linsebigler, A. L., Lu, G., and Yates, J. T. Jr. (1995). Photocatalysis on TiO₂ surfaces: principles, mechanisms, and selected results. **Chemical Review** 95: 735-758.
- Makov, G. and Payne, M. C. (1995). Periodic boundary conditions in *ab initio* calculations. **Physical Review B** 51: 4014-4022.
- Methfessel, M. and Paxton, A. T. (1989). High-precision sampling for Brillouin-zone integration in metals. **Physical Review B** 40: 3616-3621.
- Mikami, M., Nakamura, S., Kitao, O., and Arakawa, H. (2002). Lattice dynamics and dielectric properties of TiO₂ anatase: A first principles study. **Physical Review B** 66: 1552131.
- Mills A. and Hunte, S. L. (1997). An overview of semiconductor photocatalysis. **Journal of Photochemistry and Photobiology A: Chemistry** 108: 1-35.
- Mo, S. D. and Ching, W. Y. (1995). Electronic and optical properties of three phases of titanium dioxide: Rutile, anatase, and brookite. **Physical Review B** 51: 13023-13032.
- Monkhorst, H. J. and Pack, J. D. (1976). Special points for Brillouin-zone integrations **Physical Review B** 13: 5188-5192.

- Muscat, J., Swamy, V., and Harrison, N. M. (2002). First-principles calculations of the phase stability of TiO₂. **Physical Review B** 65: 224112-224126.
- Na-Phattalung, S., Smith, M. F., Kim, K., Du, M. H., Wei, S. H., Zhang, S. B., and Limpijumngong, S. (2006). First-principles study of native defects in anatase TiO₂. **Physical Review B** 73: 125205.
- Nerlov, J., Qingfeng, G., and Møller, P. J. (1996). Resonant photoemission from TiO₂ (110) surfaces: Implications on surface bonding and hybridization. **Surface Science** 348: 28-38.
- Neugebauer, J. and Van de Walle, C. G. (1994). Atomic geometry and electronic structure of native defects in GaN. **Physical Review B** 50: 8067-8070.
- Ortiz, G. and Ballone, P. (1991). Pseudopotentials for non-local-density functionals. **Physical Review B** 43: 6376-6387.
- Northrup, J. E. and Zhang, S. B. (1994). Energetics of the As vacancy in GaAs: The stability of the 3+ charge state. **Physical Review B** 50: 4962-4964.
- Park, B. H., Huang, J. Y., Li, L. S., and Jia, Q. X. (2002). Phase control of epitaxial TiO₂ films grown by pulsed laser deposition. **Applied Physics Letter** 80: 1174.
- Parker, R. A. (1961). Static Dielectric Constant of Rutile (TiO₂), 1.6-1060°K. **Physical Review** 124: 1719-1722.
- Payne, M. C., Teter, M. P., Allan, D. C., Arias, T. A., and Joannopoulos, T. A. (1992). Iterative minimization techniques for *ab initio* total-energy calculations: molecular dynamics and conjugate gradients. **Reviews of Modern Physics** 64: 1045-1097.

- Perdew, J. P., Burke, K., and Ernzerhof, M. (1996). Generalized Gradient Approximation Made Simple. **Physical Review Letter** 77: 3865-3868.
- Perdew, J. P. and Wang, Y. (1986). Accurate and simple density functional for the electronic exchange energy: Generalized gradient approximation. **Physical Review B** 33: 8800-8802.
- Perdew, J. P. and Wang, Y. (1993). Accurate and simple analytic representation of the electron-gas correlation energy. **Physical Review B** 45: 13244-13249.
- Perdew, J. P. and Zunger, A. (1981). Self-interaction correction to density-functional approximations for many-electron systems. **Physical Review B** 23: 5048-5079.
- Sasaki, J., Peterson, N. L., and Hoshino, K. (1985). **Journal of Physics and Chemistry of Solids** 46: 1267; and references therein.
- Stibor, A. (2001). **CO adsorption on iron surfaces: An ab-initio density-functional study** [On-line].
Available: <http://homepage.univie.ac.at/alexander.stibor/Diplomarbeit.pdf>
- Sullivan, J. M. and Erwin, S. C. (2003). Theory of dopants and defects in Co-doped TiO₂ anatase. **Physical Review B** 67: 144415-144421.
- Thomas, L. H. (1927). The calculation of atomic fields. **Proceedings of the Cambridge Philosophical Society** 23: 542-548.
- Van de Walle, C. G., and Neugebauer, J. (2004). First-principles calculations for defects and impurities: applications to III-nitrides. **Journal of Applied Physics** 95: 3851-3879
- Vanderbilt, D. (1990). Soft self-consistent pseudopotentials in a generalized eigenvalue formalism. **Physical Review B** 41: 7892-7895.

- Vosko, S. H., Wilk, L., and Nusair, M. (1980). Accurate spin-dependent electron liquid correlation energies for local spin density calculations: a critical analysis. **Canadian Journal of Physics** 58: 1200-1211.
- Watts, R. J., Kong, S., Orr, M. P., Miller, G. C., and Henry, B. E. (1995). Photocatalytic Inactivation of Coliform Bacteria and Viruses in Secondary Waste-Water Effluent. **Water Research** 29: 95-100.
- Wigner, E. P. (1938). Effects of the electron interaction on the energy levels of electrons in metals. **Transactions of the Faraday Society** 34: 678-685.
- Yaki, E., Koyama, A., Sakairi, H., and Hasiguti, R. R. (1977). **Journal of the Physical Society of Japan** 42: 939.
- Yong, X. and Martin A. A. S. (2000). The absolute energy positions of conduction and valence bands of selected semiconducting minerals. **American Mineralogist** 85: 543-556.
- Zhang, S. B. (2002). The microscopic origin of the doping limits in semiconductors and wide-gap materials and recent developments in overcoming these limits: a review. **Journal of Physics: Condensed Matter** 14: R881-R903.
- Zhang, S. B. and Northrup, J. E. (1991). Chemical Potential Dependence of Defect Formation Energies in GaAs: Application to Ga Self-Diffusion **Physical Review Letter** 67: 2339-2342.
- Zhang, S. B., Tománek, D., Cohen, M. L., Louie, S. G., and Hybertsen, M. S. (1989). Evaluation of quasiparticle energies for semiconductors without inversion symmetry. **Physical Review B** 40: 3162-3168

- Zhang, S. B., Wei, S.-H., and Zunger, A. (2001). Intrinsic *n*-type versus *p*-type doping asymmetry and the defect physics of ZnO. **Physical Review B** 63: 075205-075211.
- Zhang, Z., Jeng, S. P., and Henrich, V. E. (1991). Cation-ligand hybridization for stoichiometric and reduced TiO₂ (110) surfaces determined by resonant photoemission. **Physical Review B** 43: 12004-12011.

APPENDIX

PAPER OF PRESENTATION

First-principles study of native defects in anatase TiO₂

Sutassana Na-Phattalung,^{1,2} M. F. Smith,¹ Kwiseon Kim,³ Mao-Hua Du,³ Su-Huai Wei,³

S. B. Zhang,³ and Sukit Limpijumnong^{1,2,3}

¹*National Synchrotron Research Center, Nakhon Ratchasima, Thailand*

²*School of Physics, Suranaree University of Technology, Nakhon Ratchasima, Thailand*

³*National Renewable Energy Laboratory, Golden, Colorado 80401, USA*

(Received 21 January 2006; revised manuscript received 27 February 2006; published 31 March 2006)

Native point defects in anatase TiO₂ are investigated by using first-principles pseudopotential calculations based on density-functional theory (DFT). Antisite defects, namely, Ti-antisite (Ti_O) and O-antisite (O_{Ti}), have high formation energies and are hence unstable. In contrast, all other fundamental native defects (Ti_i, O_i, V_{Ti}, and V_O) have low formation energies. In particular, titanium interstitial Ti_i is a quadruple donor defect with lowest formation energy in *p*-type samples, whereas Ti vacancy (V_{Ti}) is a quadruple acceptor defect with lowest formation energy in *n*-type samples. Interstitial oxygen (O_i) would spontaneously and strongly bind to lattice oxygen, resulting in a neutral O₂ dimer substituting on one O site. None of the four low-energy defects have energy levels inside the DFT band gap.

DOI: 10.1103/PhysRevB.73.125205 PACS number(s): 61.72.Bb, 61.72.Ji

I. INTRODUCTION

Semiconductor photocatalysis begins with the activation of an electron from the valence band to the conduction band by optical excitation, creating an electron in the conduction band and a hole in the valence band. These excited carriers may diffuse to the surface to initiate chemical reactions with agents in the surrounding fluid. (The process is commonly applied to air and water purification, for which the relevant chemical reactions are those resulting in the destruction of various microorganisms.^{1,2}) Electron-hole recombination is an important competing process, as it tends to prevent the carriers from reaching the surface. The efficiency of a photocatalytic process involving visible light thus depends mainly on two factors: (i) the absorption of the semiconductor in the visible region, which determines the initial number of carriers being created, and (ii) the time required for the excited carrier to move to the surface to initiate reactions, as compared to the recombination lifetime. The ratio between these two time constants determines the fraction of the carriers that will take part in photocatalysis. In this regard, it is often beneficial to use small particles ranging between 1 and 100 nm in diameter to maximize the photocatalytic rates.

TiO₂ has been successfully applied as a semiconductor photocatalyst. Its main advantages over similar materials are its high oxidizing power and durability (i.e., high resistance to photo- and chemical corrosion). A major drawback of the TiO₂, however, is its large band gap, which does not permit efficient absorption of visible light and hence prevents TiO₂ from being used in large-scale environmental applications. There is a rich literature describing the attempts to chemically dope TiO₂ in order to reduce

the band gap, but how to best manipulate the gap while maintaining the beneficial photocatalytic properties is still an unresolved challenge. For example, one of the difficulties in the chemical doping is that, while reducing the band gap, the dopants also act as carrier scattering centers and traps, which reduce the chance for the carriers to reach particle surfaces to participate in the desired reactions. Further complications arise in an effort to distinguish the effect of surface impurities from that of bulk impurities. These problems underscore the need to understand, in detail, the changes in TiO_2 that result from impurity introduction. Before this can be done, however, one also has to understand the role of native defects in TiO_2 . Native defects could influence both of the factors mentioned above. The concentration of the native defects typically depends on the growth conditions, as well as on the presence of chemical impurities. This implies that it will be difficult for an experimentalist to unravel the effect of a particular chemical impurity simply from measuring the doping dependence of a photocatalytic process, because it is difficult to get rid of all the native defects. It is therefore desirable to study the properties of the defects. At the very least, one should know what can be expected under the various growth conditions, so that the experimental results can be interpreted without any ambiguity arising from the contribution of the native defects.

TiO_2 has three polymorphs: rutile, anatase, and brookite. Rutile TiO_2 is the most studied phase. This is probably due to its simple crystal structure and to the fact that rutile single crystal, as well as thin film can be readily grown by several conventional techniques. Brookite TiO_2 is the least studied TiO_2 , due to its complex structure and naturally the difficulties encountered during growth. Although bulk single-crystal anatase is less stable than bulk rutile, nanoparticles of TiO_2 used in photocatalysis and photoelectrochemistry³ tend to exhibit only the anatase structure. For this reason, we will consider here the anatase polymorph. To our knowledge, no first-principles studies of native point defects in any form of the TiO_2 have previously been carried out.

Using first-principles total-energy calculations, we have investigated the fundamental native point defects in anatase TiO_2 . These include Ti vacancy (V_{Ti}), O vacancy (V_{O}), Ti interstitial (Ti_i), and O interstitial (O_i). All can have very low, and even negative, formation energies depending on the growth conditions. We have also studied the antisites and found that they have very high energies due to the large cation-anion size mismatch and strong ionicity of TiO_2 (see Table I). The formation energy of an antisite is even higher than the sum of those for vacancy and interstitial. For instance, the energy of O_{Ti} is higher than the sum of V_{Ti} and O_i . This means O_{Ti} is unstable against spontaneous disintegration into a pair of isolated V_{Ti} and O_i . Since antisites are unlikely to form in TiO_2 , they are excluded from the discussion below. Due to a strong preference of the interstitial O_i to bind strongly with lattice O, however, a substitutional diatomic molecule (O_2) always forms on the O site. To be consistent with our earlier work of defects in ZnO, we will call this paired oxygen (O_2)_O.⁴

Interestingly, none of the above defects has a level inside the density functional theory (DFT) band gap. This finding is unexpected because, typically, native defects in wide gap semiconductors⁵⁻⁷ do introduce deep levels inside the DFT gaps. Later in the paper we will present a simple qualitative picture to show why the more ionic TiO_2 is distinct from other semiconductors in this way.

TABLE 1 Formation energy of native defects in anatase TiO₂ with the Fermi level at the VBM. The results are shown for both the 48- and 108-atom supercells. Both the Ti-rich ($\mu_{\text{Ti}} = -2.67$ eV, *precipitated by* Ti₂O₃; $\mu_{\text{O}} = -3.79$ eV) and O-rich ($\mu_{\text{Ti}} = -10.25$ eV; $\mu_{\text{O}} = 0$ eV) conditions are shown.

Defect	Charge state	E_f (eV) (Ti-rich ^a)		E_f (eV) (O-rich)	
		48-atom	108-atom	48-atom	108-atom
Ti _i	+4	-9.88	-9.42	-2.32	-1.84
V _{Ti}	-4	12.64	13.40	5.06	5.82
O ₂ ≡ (O ₂) _O	0	4.50	4.40	0.71	0.61
V _O	+2	-2.82	-3.29	0.97	0.52
O _{Ti}	-4		21.91		10.54
Ti _O	+6		-6.83		4.53

^aFor Ti-rich case, we have taken into account the formation of Ti₂O₃, which has a lower energy than the Ti metal

II. COMPUTATIONAL METHOD

We used the DFT with the local density approximation (LDA) and ultrasoft pseudopotentials, 8 as implemented in the VASP codes.⁹ The cutoff energy for the plane-wave basis set is 300 eV. Our calculated crystal parameters of bulk anatase TiO₂ are $a=3.764$, $c/a=2.515$, and $u=0.208$. These are in good agreement with the experimental values: $a=3.785$, $c/a=2.513$, and $u=0.208$ (Ref. 10). Other calculations¹¹⁻¹³ showed similar agreement. To calculate the formation energy of the defects, a supercell approach is used^{14,15} in which all atoms are allowed to relax by minimization of the Hellmann-Feynman force to less than 0.05 eV/Å. Our preliminary study was based on a supercell with 48 atoms, as a 2x2x2 repetition of the primitive anatase unit cell. To ensure the convergence of the calculations, especially for high charge-state defects, we repeated all the calculations with a larger supercell size of 108 atoms (namely 3x3x2). We found that formation energies calculated using the 48-atom cell typically agree to within 0.45 eV with those calculated using the 108-atom cell (best case: (O₂)_O⁰, 0.1 eV; worst case: V_{Ti}⁴⁻, 0.76 eV). For the Brillouin zone integration, a 2×2×2 Monkhorst-Pack special k-point mesh is used regardless of the cell size. Unless noted otherwise, all results presented here are based on the 108-atom cell calculations. We will present the electronic structure using a special k -point scheme as discussed in Ref. 16. The calculated band gap averaged over the special k is 2.32 eV. Due to the well-known LDA gap error, the calculated band gap is smaller than the experimental band gap of 3.2 eV.

For a supercell, the defect formation energy is defined as¹⁴

$$E^f = E_{tot}(D^q) - E_{tot}(\text{TiO}_2, \text{bulk}) + \sum_x \Delta n_x \mu_x + qE_F, \quad (1)$$

where $E_{tot}(D^q)$ is the total energy of the cell with defect D in charge state q . $E_{tot}(0)$ is the total energy of the cell without the defect. Δn_x is the number of species X ($= \text{Ti}, \text{O}$) being removed from a defect-free cell, to its respective reservoir with chemical potential μ_x to form the defect cell. The chemical potential reflects the availability (or elemental partial pressure) of each element. During the growth, if any chemical potential rises above its natural phase value (i.e., that of hcp Ti and O_2 molecule), then the natural phase will form instead of the TiO_2 . Because of this, only the μ_x values below those of the natural phases need to be considered. More strict limitations on the chemical potentials may be further imposed by the formation of alternative phases containing both Ti and O, as will be discussed below.

If the TiO_2 crystal is to grow slowly, it is required that:

$$\mu_{\text{TiO}_2} = \mu_{\text{Ti}} + 2\mu_{\text{O}}, \quad (2)$$

where μ_{TiO_2} is the chemical potential of anatase TiO_2 . If we set $\mu_x = 0$ for their respective natural phases, then $\mu_{\text{TiO}_2} = -10.25$ eV is the calculated formation energy of anatase TiO_2 per molecular formula. The constraint, Eq. (2), ensures equilibrium growth conditions. If the sum on the right hand side is larger than μ_{TiO_2} , then the crystal will grow rapidly and will not be homogeneous. On the other hand, if this sum is lower than μ_{TiO_2} , then the crystal will disintegrate instead of grow.

In Fig. 1, we illustrate the allowable conditions of growth on a graph of μ_{Ti} versus μ_{O} . The condition given by Eq. (2) is indicated by a solid line. There are other titanium-oxygen stable phases that may exist, including Ti_2O_3 and TiO . Since the Ti-to-O ratio is higher in both Ti_2O_3 and TiO than that in TiO_2 , we expect the growth of these alternate phases to be favorable under the Ti-rich growth conditions. To determine whether the formation of these alternative phases imposes a stricter upper limit on μ_{Ti} , we need to consider the equilibrium growth of Ti_2O_3 and TiO . For example for Ti_2O_3 , equilibrium growth takes place when

$$\mu_{\text{Ti}_2\text{O}_3} = 2\mu_{\text{Ti}} + 3\mu_{\text{O}}, \quad (3)$$

where $\mu_{\text{Ti}_2\text{O}_3} = -16.7$ eV is the calculated formation energy of Ti_2O_3 . Equation (4.4) (and the corresponding expression for TiO) is illustrated by a dashed (and dotted) line in Figure 4.1. We see that the lines corresponding to Eqs. (2) and (3) intersect at $\mu_{\text{Ti}} = -2.67$ eV. For higher values of μ_{Ti} , the growth of Ti_2O_3 is expected to proceed much more rapidly than that of TiO_2 , so that we may regard $\mu_{\text{Ti}} = -2.67$ eV as the real upper limit for the TiO_2 growth. With this, the range of allowable growth conditions is described by the bold solid line in Fig. 1

In our calculations, we vary the charge of the defect in order to identify the most stable charge state. To calculate the charged defects, a jellium background is used to neutralize the supercell. We have not applied any correction to the fictitious electrostatic interactions between the charged defect and its images in the neighboring supercells. This is justifiable especially in the case of TiO_2 where the dielectric constant ($\epsilon > 100$) (Ref. 18) is about an order of magnitude higher than other semiconductors. The high dielectric constant results in small correction terms for the fictitious electrostatic interactions. For instance, the leading term of the Makov-Payne correction¹⁹ for the charge state $4\pm$ in the 108-atom cell is only about 0.1 eV, which is

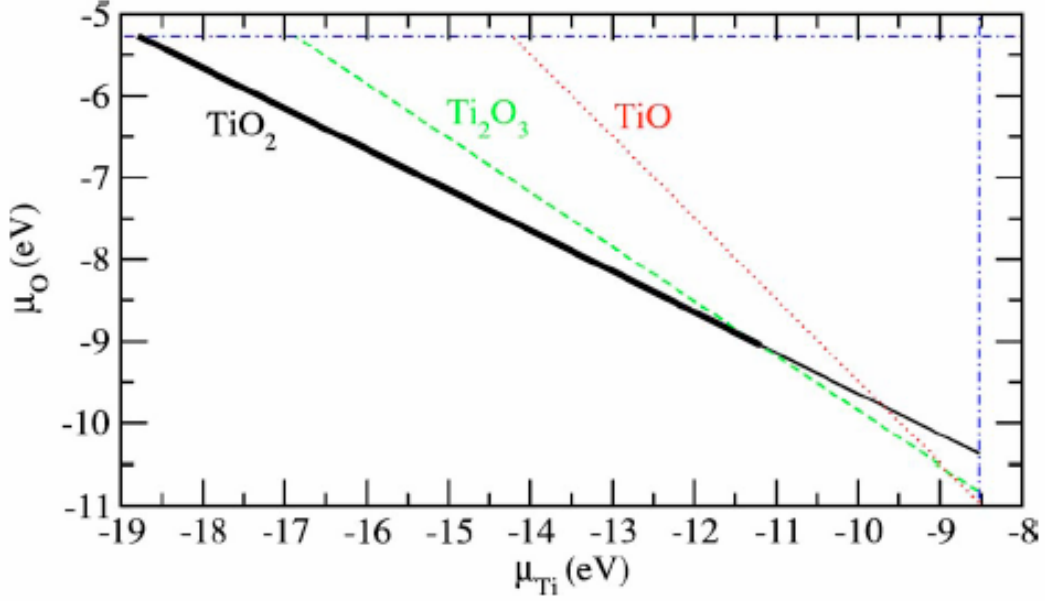


Figure 1 (Color online) Graphic illustration of thermodynamic growth conditions for TiO₂, i.e. the allowed values of the atomic chemical potentials, μ_{Ti} and μ_{O} . The dot-dashed horizontal and vertical lines indicate the upper bounds determined by the natural phases of Ti and O, respectively. Equilibrium growth of TiO₂ takes place for μ_{Ti} and μ_{O} lying on the solid line, whereas equilibrium growth of Ti₂O₃ and TiO takes place for μ_{Ti} and μ_{O} lying in the dashed and dotted lines, respectively.

comparable to the expected error bars of our calculations. Moreover, we compare the results of the 48- and 108-atom cells to estimate the errors arising from the finite cell size and the supercell shape.

The concentration of a defect (c) is related to its formation energy E^f , through the equation

$$c = N_{\text{sites}} \exp(-E^f / kT), \quad (4)$$

where N_{sites} is the number of possible lattice sites per unit volume to form the defect, k is the Boltzmann's constant, and T is the temperature in Kelvin. To be exact, Eq. (4) is only valid under thermodynamic equilibrium. Actual growth of TiO₂ (as well as other semiconductors) is usually a non-equilibrium process. This means that the concentration of a defect can deviate substantially from that given by Eq. (4). Regardless of whether the growth/anneal process is under the thermal equilibrium or not, the formation energy is still a good indicator of the abundance of the defect: namely, defects with high formation energies are difficult to be incorporated and defects with lower formation energies are more likely to form.

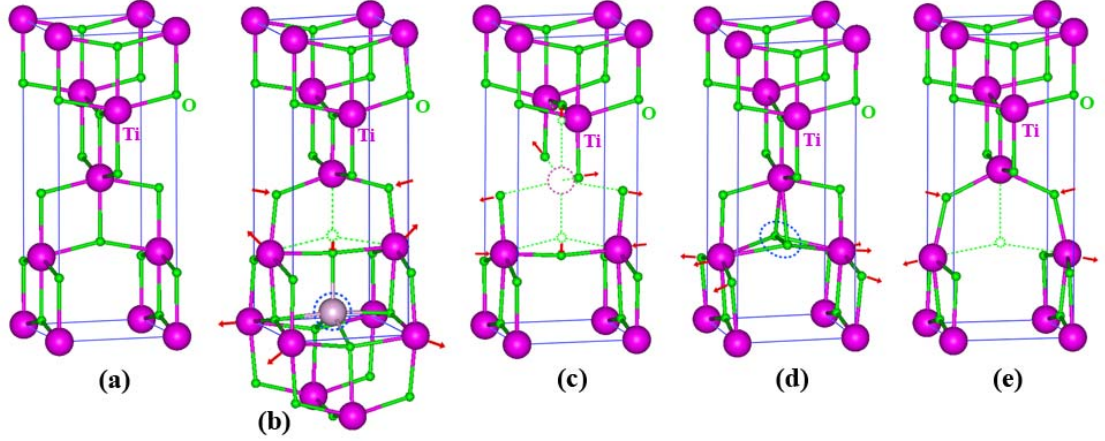


Figure 2 (Color online) Atomic structures of (a) bulk anatase TiO_2 , (b) Ti_i^{4+} , (c) V_{Ti}^{4-} , (d) $(\text{O}_2)_\text{O}$, and (e) V_O^{2+} defects. The large purple spheres are the Ti, the small green spheres are the O. Relaxation directions of neighboring atoms are selectively.

III. RESULTS AND DISCUSSION

A. Structural properties of the anatase TiO_2

TiO_2 is a highly ionic semiconductor. The strength of the Coulombic attraction between the cation and anion is decisive in determining its crystal stability. In general, an ionic crystal prefers structures that maximize the number of oppositely charged nearest neighbors for each ion. This is in contrast to covalent semiconductors, which often exhibit tetrahedral bonding configurations that allow the formation of sp^3 hybridization. In TiO_2 , the Ti atom (with a high oxidation number of +4) prefers to have a large number of O neighbors (oxidation number = -2), and strongly repels its Ti next-nearest neighbors. The specific geometry of the anatase crystal structure is such that each Ti atom has six O neighbors but only four Ti next-nearest neighbors. This explains why it is one of the stable crystal structures for TiO_2 . Since O has a smaller oxidation number than Ti, it also has a smaller number (only three) of Ti neighbors. An illustration of the anatase crystal structure is shown in Fig. 2(a). One can think of this crystal structure as obtained from a distorted NaCl structure of TiO by removing half of the Ti atoms. The slight distortion from the ideal NaCl structure results in shorter Ti-O distances and longer Ti-Ti distances to further reduce the Madelung energy.

B. Formation energies and charge states of the native defects

Figure 2 shows the calculated atomic structures of Ti_i , V_{Ti} , $(\text{O}_2)_\text{O}$, and V_O . The defect formation energies are tabulated in Table I, as well as plotted as a function of the electron Fermi energy in Fig. 3. The most important feature of Fig. 3 is that none of the defects introduce any defect levels inside the band gap. The charge state of Ti_i , V_{Ti} , $(\text{O}_2)_\text{O}$, and V_O is $4+$, $4-$, 0 , and $2+$, respectively.²⁰ Moving the Fermi level across the band gap cannot change the charge state of these defects. Even if the Fermi level is moved into the valence or conduction band, there is still no significant filling of the defect, because the defect-induced electronic states are all delocalized resonant states,

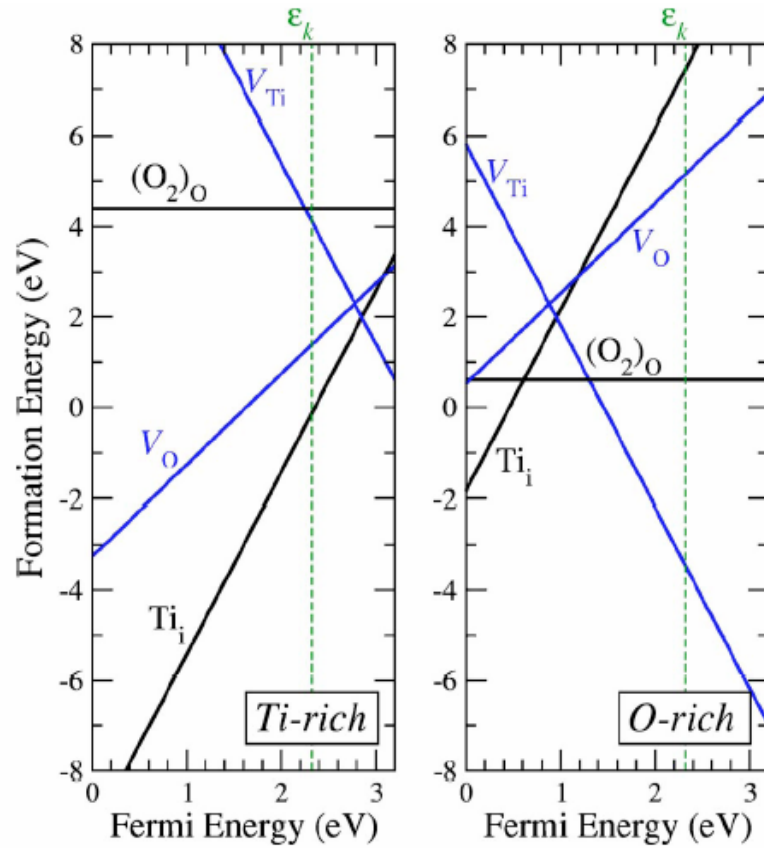


Figure 3 (Color online) Defect formation energies as a function of the Fermi level, under the Ti-rich (left panel) and O-rich (right panel) growth conditions, respectively. The slope of the line is an indication of the charge state of the defect. The Fermi energy, referenced to the top of valence band, is all the way to the experimental band gap. The vertical dotted line is the calculated bandgap at the special k -point.

as revealed by the partial DOS in Fig. 4²¹ As a result, none of these defects is a carrier trap.

Due to the well-known LDA gap problems, our calculated conduction-band minimum at the special k -points (ϵ_k) used for the Brillouin zone integration, indicated in Fig. 3 by the dashed line, is smaller than the experimental gap. However, the defect states shown in Fig. 4 are not expected to fall into the band gap when a band-gap correction is applied, because they are all delocalized resonant states with symmetries resembling those of the extended band states (i.e., both the donors [Ti_i and V_O] and conduction-band edge states have the Ti d character, while both the acceptors [$(O_2)_O$ and V_{Ti}] and valence-band edge states have the O p character), which should follow the band edge closely in schemes that correct the LDA band gap. In this regard, a GW quasiparticle calculation like the one in Ref. 22 is highly desirable to confirm such predictions.

Being free of native-defect-induced gap states is a result of high ionicity of the TiO_2 . The Ti has a small electronegativity (Ti=1.54 in Pauling scale), smaller than the cations in all major group IV, III-V, and II-V semiconductors, and the O has a very large electronegativity of 3.44. The defect states for Ti_i and V_O are the Ti d states.

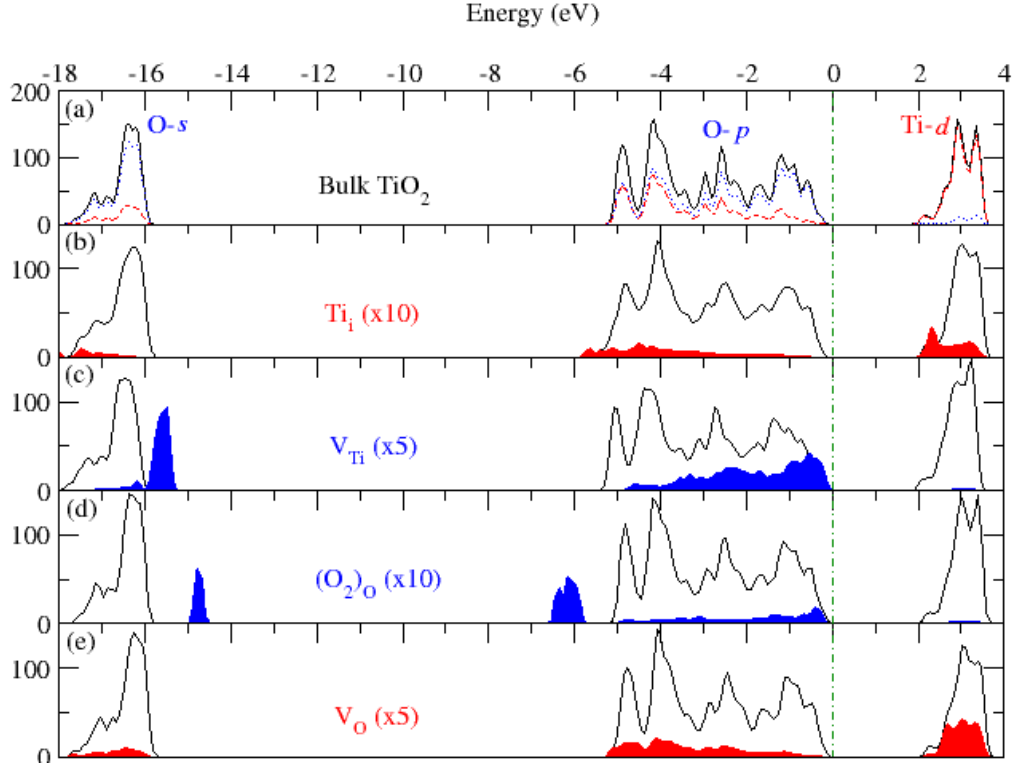


Figure 4 (Color online) Site decomposed electron density of states (DOS). For each atom center, the local partial DOS in a sphere radius R (Ti: $R = 1.48 \text{ \AA}$ and O: $R = 0.74 \text{ \AA}$) is calculated. (a) Bulk TiO_2 where solid line is the total DOS, dashed line is the DOS on Ti, and dotted line is the DOS on O. (b-e) Native defects where the shaded area is the DOS on the atoms directly related to the defect (scaled up by a factor given

Figures 4(b) and 4(e) show that these states are all above the CBM. In fact, a nominal Ti ion also has levels above the CBM. These explain why Ti_i and V_O do not induce gap levels and, as a matter of course, the large heat of formation of TiO_2 (-10.25 eV , see Sec. II). Also due to the strong electron donating tendency of Ti, the O atoms around a V_{Ti} can easily draw electrons, resulting in defect states below the VBM. Also due to the strong electron donating tendency of Ti, the O atoms around a V_{Ti} can easily draw electrons, resulting in defect states below the VBM.

C. Structure and stability of the native defects

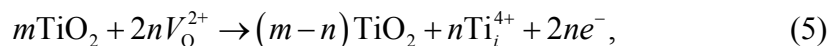
(1) Titanium interstitial (Ti_i)

Titanium interstitial favors an octahedral site [Figure 2(b)]. The site is similar to a lattice Ti site in that horizontally there are four neighboring O atoms near in a plane. The main difference is that the lattice Ti site also has two additional O atoms (one located directly above and one below). The B site places in the center of space and has five O neighbor atoms. The B site has four O neighbor atoms in diagonal axis (Ti-O distances of B site are longer than A site) and one O neighbor atom in vertical axis (located directly above). After relaxed the Ti_i in both A and B site will move to the same position [as shown in Figure 2(b)]. In the other words, after relaxed they are

the same defect. One of the vertical O neighbors moves considerably towards it. The surrounding Ti atoms are also slightly relaxed outward, due to the electrostatic repulsion between positively charge Ti ions.

Ti_i is a *quadruple shallow donor*. Under the Ti-rich and *p*-type condition, i.e., E_F is at the VBM, which is the extremely favorable situation for Ti_i^{4+} incorporation, the formation energy of the Ti_i is negative and, surprisingly, very low, i.e. -9.42 eV. This low formation energy is due mainly to the energy gain from a transfer of four electrons to the low E_F level. In addition, the anatase structure contains a lot of open space that can accommodate the interstitial atom without much strain. (First principles studies of SnO_2 also found Sn_i^{4+} to have a negative formation energy at the cation-rich and *p*-type condition.²³) This Ti_i formation energy remains to be negative as long as $E_F < 2.4$ eV (Fig. 3, left panel). A negative formation energy means that the formation of the defect is spontaneous, so it is impossible to grow TiO_2 under such conditions. (Even if one begins in the *p*-type region, the rapid formation of the quadruple donor Ti_i would quickly turn the sample *n*-type.) Under the O-rich condition, Ti_i may also have a negative formation energy unless $E_F > 0.5$ eV (see Fig. 2, right panel). From these results, we expect it to be difficult to dope TiO_2 *p*-type under any equilibrium growth conditions.

The low formation energy of Ti_i makes it the strongest candidate for the shallow donors observed in undoped anatase TiO_2 with high purity.²⁴ The low formation energy may also explain the earlier observations of Ti_i in oxygen-deficient rutile samples by ion beam channeling,²⁵ electron paramagnetic experiment,²⁶ and others as summarized in the review in Ref. 27. Although most of the experimental works were performed on rutile TiO_2 , the local structures of rutile and anatase are very similar. Because the oxygen-deficient TiO_2 samples were prepared by heating TiO_2 (1000-1400 °C) in a reducing atmosphere for an prolonged period of time (typically 100-1000 hours), it is likely that some of the O atoms first migrate out of the sample; leaving vacancies behind. However, due to the small formation energy of Ti_i , these oxygen vacancies will subsequently react with remaining TiO_2 via the following reaction:



to produce Ti_i interstitials.

(2) Titanium vacancy (V_{Ti})

The atomic structure of V_{Ti} is shown in Figure 4.2(c) As one Ti atom is missing here, the surrounding O atoms relax outward; each to a point approximately halfway between its two remaining Ti neighbors. This relaxation increases the Coulomb binding by reducing the Ti-O distances while increasing the O-O distances.

The Ti vacancy is a *quadruple shallow acceptor*. Under the O-rich (i.e. Ti-poor) growth conditon, the formation energy of V_{Ti} is negative if $E_F > 1.46$ eV. This means that V_{Ti} will spontaneously form and, as a result (and because V_{Ti} is a quadruple acceptor), E_F will be pushed down until it is below 1.46 eV. Under the Ti-rich condition, V_{Ti} is still a low-energy defect, and hence, acts as a leading native acceptor. To the best of our knowledge, there is still no experimental identification of the V_{Ti} .

(3) Oxygen interstitial (O_i)

Isolated interstitial O has high formation energy and is hence unstable. It spontaneously binds with an O on the lattice site, forming a substitutional O_2 molecule, $(O_2)_O$. Each lattice O atom has an oxidation number of -2. A neutral $(O_2)_O$ thus contains two more electrons compared to a free O_2 molecule in the vacuum. Similar to the case of substitutional diatomic molecules in ZnO,⁴ the additional two electrons occupy and completely fill the molecular $pp\pi^*$ states, which lie below the VBM. The atomic structure of the $(O_2)_O$ is shown in Figure 2(d). Because the charge neutral O_2 is electrostatically equivalent to any O atom on a lattice site, one can expect that there should not be any large relaxation of the neighboring atoms. All the neighboring Ti atoms relax only slightly outward. Substitutional O_2 has a bond length of 1.46 Å, which is very similar to substitutional O_2 in ZnO [also 1.46 Å (Ref. 4)]. The bond length of a substitutional O_2 is longer than that of a free O_2 (1.23 Å (Ref. 28)) due mainly to the occupation of the two extra electrons on the $pp\pi^*$ *antibonding* orbital, and to the screening effect of the host. Under the Ti-rich condition, the $(O_2)_O$ has high formation energy and is hence unlikely to exist in any appreciable amount. However, under the O-rich condition, its formation energy is reasonably low, making it an important defect.

(4) Oxygen vacancy (V_O)

For O vacancy, each of the three nearest neighbor Ti atoms moves away from the vacancy toward its five remaining O neighbors, as illustrated in Figure 4.2(e). The next nearest neighbor O atoms move slightly inward due to the absence of electrostatic repulsion by the missing O atom.

Our calculations show that V_O is a *double donor*. This is because the O has an oxidation state 2- or, in other words, has two additional electrons transferred from the three surrounding Ti atoms. When the oxygen is removed as a neutral atom, the two additional electrons are no longer needed, making the V_O a double donor. This is consistent with first principles calculations by Sullivan and Erwin.²⁹ The formation energy of the V_O reported in Ref. 29) is slightly higher than ours, partly because they used the “Makov-Payne correction”¹⁹).

Our calculation suggests that V_O is *not* a dominant native defect *near equilibrium growth conditions*. Even in the Ti-rich growth condition, which is most favorable for V_O formation, Ti_i has a lower formation energy than V_O at all possible E_F . However, V_O can be created in certain processes such as the annealing to create oxygen-deficient samples. Although the energetics suggests that subsequent conversion to Ti_i via Eq. (5) is likely, the kinetics may not support such a process, as one only needs to break the Coulomb bindings with three neighboring Ti to free an O, but six such bindings to free a Ti. This might be why V_O are still observed by certain experiments (thermogravimetric) electrochemical titration, diffusion, and conductivity measurements as discussed in Ref. 27).

IV. Conclusion

Our calculations of native defects in anatase TiO_2 provide detailed information on the atomic structures and electronic properties for each of them. We found that Ti_i is a quadruple donor with very low formation energy, especially in *p*-type samples but also in *n*-type samples. This makes it the strongest candidate responsible for the native *n*-type conductivity observed in TiO_2 . While V_O has higher formation energy than that

of Ti_i , the kinetic barrier for creating V_O from a perfect TiO_2 is expected to be lower than that for creating Ti_i . Hence, post-growth formation of V_O is also possible, especially after the sample has been heated for a prolonged time. A quadruple acceptor V_{Ti} is the lowest energy acceptor in TiO_2 . Thus in undoped samples, Ti_i and V_{Ti} should be the leading donor and acceptor, respectively. Formation of Ti_i is further enhanced under the Ti-rich growth condition, while that of V_{Ti} is further enhanced under the O-rich growth condition. Interstitial oxygen would spontaneously bond to lattice oxygen, forming electrically inactive O_2 dimer substituting on one O lattice site. Antisite defects have relatively high formation energies and are likely to spontaneously break into isolated vacancies and interstitials. Our calculations also show that none of the four low-energy defects, Ti_i , O_i , V_{Ti} , and V_O , introduce any defect levels inside the DFT band gap.

ACKNOWLEDGMENTS

This work was supported by the National Synchrotron Research Center (Thailand) under Contract No. 2547/004. The work at NREL was supported by the U.S. DOE under Contract No. DE-AC36-99GO10337. We acknowledge R. Thongpool for bringing the problem of defects in TiO_2 to our attention. We also thank P. Reunchan and S. Jungthawan for their help with some of the calculations and S. Rujirawat and N. Kopidakis for fruitful discussions.

-
- ¹M. R. Hoffmann, S. T. Martin, W. Choi, and D. W. Bahnemann, Chem. Rev. Washington, D.C.) **95**, 69 (1995) and references therein.
- ²J. C. Yu, J. Yu, W. Ho, Z. Jiang, and L. Zhang, Chem. Mater. **14**, 3808 (2002).
- ³Q. Chen and H.-H. Cao, THEOCHEM **723**, 135 (2005).
- ⁴S. Limpijumnong, X. Li, S.-H. Wei, and S. B. Zhang, Appl. Phys. Lett. **86**, 211910 (2005).
- ⁵S. Limpijumnong and C. G. Van de Walle, Phys. Rev. B **69**, 035207 (2004).
- ⁶J. Neugebauer and C. G. Van de Walle, Phys. Rev. B **50**, R8067 (1994).
- ⁷S. Limpijumnong, S. B. Zhang, S.-H. Wei, and C. H. Park, Phys. Rev. Lett. **92**, 155504 (2004); A. F. Kohan, G. Ceder, D. Morgan, and C. G. Van de Walle, Phys. Rev. B **61**, 15019 (2000).
- ⁸D. Vanderbilt, Phys. Rev. B **41**, R7892 (1990).
- ⁹G. Kresse and J. Furthmüller, Comput. Mater. Sci. **6**, 15 (1996).
- ¹⁰C. J. Howard, T. M. Sabine, and F. Dickson, Acta Crystallogr., Sect. B: Struct. Sci. **47**, 462 (1991).
- ¹¹A. Fahmi, C. Minot, B. Silvi, and M. Causá, Phys. Rev. B **47**, 11717 (1993).
- ¹²R. Asahi, Y. Taga, W. Mannstadt, and A. J. Freeman, Phys. Rev. B **61**, 7459 (2000).
- ¹³M. Calatayud, P. Mori-Sánchez, A. Beltrán, A. M. Pendás, E. Francisco, J. Andrés, and J. M. Recio, Phys. Rev. B **64**, 184113 (2001).
- ¹⁴S. B. Zhang and J. E. Northrup, Phys. Rev. Lett. **67**, 2339 (1991); J. E. Northrup and S. B. Zhang, Phys. Rev. B **50**, 4962 (1994).
- ¹⁵S. B. Zhang, S.-H. Wei, and A. Zunger, Phys. Rev. B **63**, 075205 (2001).
- ¹⁶S. B. Zhang, J. Phys.: Condens. Matter **14**, R881 (2002).

- ¹⁷H. Tang, H. Berger, P. E. Schmid, F. Lévy, and G. Burri, *Solid State Commun.* **23**, 161 (1977).
- ¹⁸R. A. Parker, *Phys. Rev.* **124**, 1719 (1961)
- ¹⁹G. Makov and M. C. Payne, *Phys. Rev. B* **51**, 4014 (1995)
- ²⁰The reported stable charge states of +1 and 0 for VO [J. M. Sullivan and S. C. Erwin, *Phys. Rev. B* **67**, 144415 (003)] are probably due to electron filling of the conduction-band edge states rather than the actual defect states, because their calculated transition levels are > 2.6 eV above the VBM and are hence above our calculated CBM (they have used a very similar calculation method to ours).
- ²¹For vacancies, the defect atoms include the nearest neighbors of the missing atom, i.e., six O atoms for V_{Ti} and three Ti atoms for V_O . For Ti_i , only the interstitial Ti atom itself is included as the defect atoms, whereas for $(O_2)_O$, both O atoms in the dimer are included.
- ²²S. B. Zhang, D. Tománek, M. L. Cohen, S. G. Louie, and M. S. Hybertsen, *Phys. Rev. B* **40**, 3162 (1989).
- ²³C. Kiliç and A. Zunger, *Phys. Rev. Lett.* **88**, 095501 (2002).
- ²⁴L. Forro, O. Chauvet, D. Emin, L. Zuppiroli, H. Berger, and F. Lévy, *J. Appl. Phys.* **75**, 633 (1994).
- ²⁵E. Yaki, A. Koyama, H. Sakairi, and R. R. Hasiguti, *J. Phys. Soc. Jpn.* **42**, 939 (1977).
- ²⁶M. Aono and R. R. Hasiguti, *Phys. Rev. B* **48**, 12406 (1993); R. R. Hasiguti and E. Yagi, *ibid.* **49**, 7251 (1994).
- ²⁷J. Sasaki, N. L. Peterson, and K. Hoshino, *J. Phys. Chem. Solids* **46**, 1267 (1985), and references therein.
- ²⁸K. P. Huber and G. Herzberg, *Molecular Spectra and Molecular Structure. IV. Constants of Diatomic Molecules* (Van Nostrand Reinhold, New York, 1979).
- ²⁹J. M. Sullivan and S. C. Erwin, *Phys. Rev. B* **67**, 144415 (2003).

CURRICULUM VITAE

SUTASSANA NA PHATTALUNG

Born: September 12, 1981, Nakhon Phanom

Citizenship: Thailand

Education:

1999 – 2002 B.Sc. Physics

Khonkaen University, Khonkaen, Thailand

Presentation:

1. Oral presentation at 1st Siam Physics Congress 2006, 23-25 March 2006, The Tide Resort, Bang Sean, Chonburi, Thailand.
2. Oral presentation at 1st National Symposium on Physics Graduate Research, 29 June - 1 July 2006, Chulabhorn Dam, Chaiyapum, Thailand.